vol. 174, no. 4 the american naturalist october 2009

E-Article

Recruitment in Tropical Tree Species: Revealing Complex Spatial Patterns

Thorsten Wiegand,* Isabel Martínez, and Andreas Huth

UFZ Helmholtz Centre for Environmental Research–UFZ, Department of Ecological Modeling, PF 500136, D-04301 Leipzig, Germany

Submitted September 2, 2008; Accepted March 26, 2009; Electronically published August 19, 2009

abstract: Seed dispersal should leave a signature on the spatial distribution of recruits that can be quantified using sophisticated techniques of spatial pattern analysis. Here we study spatial patterns of five frugivore-dispersed tropical tree species at the Barro Colorado Island forest, Panama, to describe detailed properties of the spatial patterns of recruits and to investigate whether these patterns were produced by temporally consistent mechanisms. Our spatial point pattern analyses detected the existence of surprising spatial structures, such as double-cluster and superposition patterns, and they allowed for a detailed quantification of their properties. The spatial recruitment patterns were composed of two independent components comprising a random component and a component showing a complex spatial pattern with two critical scales of clustering. The analysis allowed an estimation of the relative contribution of scatter dispersal versus clump dispersal in effective seed dispersal for our study species. Additionally, the cluster characteristics were temporally consistent over 25 years and correlated with several species traits. We are just beginning to discover the richness of spatial patterns found at tropical forests, and we are confident that a combination of advanced point pattern analysis with field data will allow for significant advances in establishing the link between spatial patterns and processes.

Keywords: BCI tropical forest, dispersal, point pattern analysis, pair-correlation function, multiple clustering, spatial statistics.

Introduction

The analysis of spatial patterns and processes has become increasingly important in ecological research (e.g., Pacala 1997; Tilman and Kareiva 1997; Bolker and Pacala 1999; Murrell et al. 2001; Amarasekare 2003). Interest in studying spatial patterns has been fueled by advances in coexistence theory showing that several mechanisms related to aggregated spatial patterns may promote species coexistence in plant communities (e.g., Hurtt and Pacala 1995; Chesson 2000; Hubbell 2001; Schupp et al. 2002). Aggregated spatial patterns are common in tropical forests (Condit et al. 2000), and many different mechanisms may cause this aggregation; for example, (1) dispersal limitation causes clumps of recruits that do not correspond to topography (Condit et al. 2000; Plotkin et al. 2000), (2) contagious seed dispersal by animals that visit determinate feeding roosts, latrines, or sleep trees may cause recruits to grow close together (e.g., Howe 1989; Fragoso 1997; Schupp et al. 2002; Fragoso et al. 2003; Kwit et al. 2007), or (3) forest gaps may imprint clumped distributions of recruits of pioneer species (e.g., Hubbell et al. 1999).

Another motivation for studying spatial patterns is that they may conserve an imprint of past processes, constituting an ecological archive from which we may recover information about the underlying processes (Wiegand et al. 2003; Grimm et al. 2005; McIntire and Fajardo 2009). However, this is challenging because the underlying processes may be complex, for example, involving multispecies trophic interactions (Fragoso 2005), because several processes may modify the spatial patterns of plants in their transition from seed to adult (Russo and Augspurger 2004) and because the same types of patterns may be generated by substantially different processes (Levin 1992; Barot et al. 1999; Wiegand et al. 2003; McIntire and Fajardo 2009). We argue that techniques of spatial pattern analysis employed in ecology have often been too simple to characterize spatial patterns in enough detail to be able to relate them to processes (McIntire and Fajardo 2009). For example, recent studies in tropical forests have assigned only a single scale of aggregation to each species (e.g., Condit et al. 2000; Plotkin et al. 2002; Seidler and Plotkin 2006), and we are just beginning to explore spatial patterns that show aggregation at several scales.

Wiegand et al. (2007*a*) developed techniques that allow for a sophisticated analysis of clustered spatial patterns. By analyzing the spatial pattern of *Shorea congestiflora*, a dominant species in the 25-ha Forest Dynamics Plot in a rain forest at Sinharaja (Sri Lanka), they made an unexpected observation. The spatial pattern of juveniles of this species turned out to be a superposition of two independent patterns: a random pattern and a pattern that showed clustering at two critical scales. The existence of two in-

* Corresponding author; e-mail: thorsten.wiegand@ufz.de.

Am. Nat. 2009. Vol. 174, pp. E106–E140.
DOI: 10.1086/605368

dependent juvenile plant subpopulations within the same species must have a mechanistic explanation, since it is quite unlikely that it may arise just by chance. One explanation is that two dispersal mechanisms exist, one of which promotes a scattered distribution of seeds while the other is involved in the creation of seed clumps.

Howe (1989) pointed to two contrasting seed deposition patterns of animal-dispersed tree species: scatter dispersal and clump dispersal. The behavior of frugivores such as small birds or bats that regurgitate, spit, or defecate seeds singly may lead to isolated recruits. Conversely, large frugivores that defecate seeds in masses may cause aggregated recruit patterns (Howe 1989). Additionally, secondary dispersal by central-place foragers such as ants may increase clumping of seed deposition by depositing seeds from a wide area within a nest or a refuse pile (Passos and Oliveira 2002). Scattered versus clustered seed deposition may occur for plant species with a diverse assemblage of dispersers, but this can even be caused by two different behavioral patterns in a single frugivore species (e.g., Russo and Augspurger 2004). Such differences in seed deposition behavior should imprint a signature in spatial patterns that would remain undetected when standard methods are used. However, detecting superposition of different dispersal modes is of prime importance in order to better understand regeneration and to develop appropriate seed dispersal kernels (Russo et al. 2006).

More generally, the question of how to link the dispersal mechanisms with the spatial processes that they generate is one of the large, persistent challenges of seed dispersal biology (Clark et al. 1999*a*; Nathan and Muller-Landau 2000). Three approaches have advanced this endeavor. Inverse modeling (Ribbens et al. 1994; Clark et al. 1999*b*) reconstructs dispersal kernels from the spatial patterns of mother trees and seeds, forward prediction of spatial patterns directly models the behavior of the seed dispersal agent (e.g., wind, primates, birds; Russo et al. 2006), and backward predictions use only spatial statistics on the pattern of recruits (Wiegand et al. 2007*a*).

In this article we focus on the approach of spatial statistics. Fitting complex point process models with two critical scales of aggregation allows us to extract detailed characteristics of the recruitment patterns, and our method is able to separate the spatial pattern of recruits stemming from scattered versus clustered seed deposition mechanisms. The basic idea is that a detailed description of the characteristics of the spatial pattern of recruitment may help, in concert with data on species traits, to infer the underlying processes (McIntire and Fajardo 2009). More specifically, we analyzed the spatial recruitment pattern of five tree species at the seasonally moist tropical forest on Barro Colorado Island (BCI; Panama). These tree species were the subject of a detailed study by Wehncke et al. (2003) analyzing seed dispersal by white-faced capuchin monkeys (*Cebus capucinus*).

We performed three groups of analyses. The objective of our first analysis was to investigate whether the recruitment patterns comprised a random component that was superposed by a second, clustered component (Wiegand et al. 2007*a*). Second, we investigated the temporal component of the spatial pattern of recruits by analyzing the data of different forest censuses (i.e., 1985, 1990, 1995, 2000, and 2005) separately. Our objectives here were to determine whether the cluster characteristics were temporally consistent and whether recruitment patterns of different census periods were spatially dependent (which would indicate temporally persistent regeneration hotspots; Hampe et al. 2008). The objective of our third analysis was to assess the possible role of dispersal limitation. If this mechanism is involved in the creation of clustering, we would expect recruits to cluster around reproductive trees. Finally, we related the fitted model parameters to species traits. Our general objective was to determine to what extent the use of sophisticated techniques of pattern analyses, in concert with one of the best field data sets available for tropical forests, allows the inference of processes from spatial patterns.

Methods

Study Site and Study Species

The forest site we studied is the 50-ha (500 m × 1,000 m) Forest Dynamics Plot (FDP) at BCI (9°10′N, 79°51′W; Hubbell et al. 1999). BCI has a moist, lowland, tropical climate, with 2,500 mm of rain per year, a strong 3.5-month dry season, and a year-round mean daily temperature of 27°C (Leigh 1999). The island is covered by tall, high-biomass forest. Censuses were first performed in 1982, and they have been repeated every 5 years since 1985. All free-standing woody stems in the plot that were ≥1 cm diameter at breast height (DBH) were tagged, mapped, and identified to species, and the DBH was recorded to the nearest millimeter. The plot is described in detail by Hubbell and Foster (1983), and details on census methods can be found in Condit (1998).

We used data from all six censuses (i.e., 1981–1983, 1985, 1990, 1995, 2000, and 2005; Hubbell et al. 2005). Our main focus was on the spatial pattern of recruits, that is, all trees that appeared for the first time in a given census t but that were not present in the previous census $t - 1$. This allowed us to define five recruitment generations for each species. For each generation t, we also looked at the pattern of potential parent trees, that is, all trees of a given species that reached reproductive size at census $t - 1$ (see table 1; Hubbell et al. 2005). Among the monkey-dispersed

Table 1: Summary of species properties

Species	Growth form[a]	Guild[a]	Maximum sapling growth rate (mm y^{-1})[b]	Minimum reproductive size (cm)[c]	Fruit type[a]	Seeds per fruit[d]	Mean seed size (mm)[e]	Median or mean distance (m)[d,f]	Dispersal agents[d,f]	Light-sensitivity coefficient[g]
Cecropia insignis	T	G	1.771	30	Achene	1,000–2,000	2.3	.8	A, P, B	1.71
Cordia bicolor	M	G	.527	16	Drupe	1	8	15.3	A, P	.53
Hasseltia floribunda	M	S	.201	8	Berry	2	5	8.9	A, P	.2
Miconia argentea	M	G	.484	10	Berry	1–80	1	51.5	A, P, ants	.48
Randia armata	U	S	.139	5	Berry	…	10	9.9	A, P, B	.14

Note: T = large tree, M = midsized tree, U = understory, G = gap, S = shade tolerant (Croat 1978); A = avian, P = primate, B = bat (Dalling et al. 2002).

[a] From Croat (1978).

[b] Given as difference in diameter at breast height (DBH; Comita et al. 2007*b*).

[c] Given as DBH (Hubbell et al. 2005).

[d] From Dalling et al. (2002).

[e] From appendix 1 in Wehncke et al. (2003).

[f] From Muller-Landau et al. (2008).

[g] Coefficient of the log-log relationship between percentage reconstructed light and number of recruits in 5 m × 5 m plots (Rüger et al. 2009).

tree species studied by Wehncke et al. (2003), we focused on five common species that were suitable for our purpose: *Cecropia insignis*, *Cordia bicolor*, *Hasseltia floribunda*, *Miconia argentea*, and *Randia armata*. *Cebus* monkeys defecated seeds in small clumps and produced overall scattered long-distance seed dispersal patterns, but other dispersers (including bats, tapirs, and howler and spider monkeys) primarily deposited seeds in clumps at feeding roosts, latrines, and sleeping trees (Wehncke et al. 2003). Some of these species experienced secondary dispersal by dung beetles, ants, and rodents (Dalling et al. 1998). The properties of the tree species are summarized in table 1.

Spatial Pattern Analysis

The data on the fully censused megaplots of tropical forests sampled within the network of the Center for Tropical Forest Science provide, for each census, a map of the location of the stems of all trees and shrubs, their DBH values, and their species identity. Spatial statistics provide a rich array of techniques to analyze such point pattern data (Stoyan and Stoyan 1994; Diggle 2003; Illian et al. 2008), which are increasingly being used in ecology (e.g., He et al. 1997; Barot et al. 1999; Wiegand et al. 1999, 2007*a*, 2007*b*, 2007*c*; Goreaud and Pelissier 2003; Wiegand and Moloney 2004; Getzin et al. 2008). Of special interest in ecology are summary statistics such as the pair-correlation function (Stoyan and Stoyan 1994; Wiegand et al. 1999; Condit et al. 2000) or the distribution function of nearest-neighbor distances (Diggle 2003), which quantify the small-scale spatial correlation structures of point patterns. An assumption of most methods of point pattern analysis is that the pattern is homogeneous, that is, it has the same properties within the entire study region. If this is not the case, specific methods are required (Baddeley et al. 2000; Wiegand et al. 2007*c*; Getzin et al. 2008; Illian et al. 2008).

The pair-correlation function $g(r)$ is a normalized neighborhood density function, and it can be defined as the expected density of trees of an average tree of the pattern at distance r, divided by the mean density λ of trees in the study region (Stoyan and Stoyan 1994). The value of the pair-correlation function for a random pattern is thus $g(r) = 1$, and clustering (i.e., an elevated tree density) is indicated by values of $g(r) > 1$. Additional information is provided by summary statistics that consider only the nearest neighbors. We used the cumulative distribution functions $D(y)$ of the distances y to the nearest neighbor (Diggle 2003; Illian et al. 2008), which gives the probability that the average tree of the pattern has its nearest neighbor within distance y. The short-sighted function $D(y)$ selectively characterizes the small-scale clustering and allows distinguishing alternative point processes with multiple scales of clustering (Wiegand et al. 2007*a*). We calculated $D(y)$ without edge correction (Diggle 2003). The univariate $g(r)$ and $D(y)$ used in the analysis of single species can be extended to bivariate functions describing the association (interaction) between two different types of trees (e.g., different species or size classes). The quantity $\lambda_2 g_{12}(r)$ represents the expected density of trees of type 2 at distance r of an average tree of type 1 (where λ_2 is the

intensity of type-2 trees), and $D_{12}(y)$ is the cumulative distribution function of the distances y from type-1 trees to their nearest type-2 neighbor.

We contrasted specific null models to our data and used a Monte Carlo approach for the construction of simulation envelopes. Each of the $n = 199$ simulations of the point process underlying the null model generates a g (or D) function, and simulation envelopes with an approximate error rate of $\alpha = 0.05$ were calculated from the fifth-highest and -lowest values of 199 simulations of the g (or D) function (Stoyan and Stoyan 1994). We evaluated the fitted cluster processes (and other null models) using a goodness-of-fit test (Diggle 2003; Loosmore and Ford 2006). This test reduces the scale-dependent information of the pair-correlation function into a single test statistic u_i, which represents the total squared deviation between the observed pattern and the theoretical results across the distances of interest. The u_i statistics were calculated for the observed data ($i = 0$) and simulated data ($i = 1, \ldots, 199$), and the rank of u_0 among all u_i was determined. If the rank of u_0 was >190 (198), the data showed a significant departure from the null model (across the distances of interest) with error rate $\alpha = 0.05$ (0.01). For all point pattern analyses, we used the grid-based software Programita (Wiegand and Moloney 2004) with a grid size of 1 m^2 to estimate the summary statistics. This is a fine enough resolution compared with the 500-m × 1,000-m size of the study plot, and it is sufficient to respond to our objectives. Details on the estimators of the pair-correlation function can be found in Wiegand and Moloney (2004).

Cluster Processes

Our approach is based on extending Thomas processes (Thomas 1949), the simplest class of cluster processes with one critical scale of clustering. Note that the cluster processes used here are phenomenological, not mechanistic, and do not provide a direct link to the underlying processes. However, we use them as benchmark processes with directly interpretable parameters to succinctly summarize detailed characteristics of the complex observed spatial patterns that can be correlated with species traits.

1. Single-cluster process (Thomas process): The construction principle behind the Thomas process is simple. It consists of a number of randomly and independently distributed clusters (fig. 1*A*, 1*B*). The position of the cluster centers follows a homogeneous Poisson process (also called complete spatial randomness [CSR]) with intensity ρ (i.e., $A\rho$ is the number of clusters in a study region of area A). Thus, the number of points that belong to a given cluster follows a Poisson distribution with mean $\mu = \lambda/\rho$ (λ is the intensity of points of the pattern). In figure 1, $\mu = 144/68 = 2.1$. The location of the points in a given cluster, relative to the cluster center, has a bivariate Gaussian distribution $h(r, \sigma)$ with variance σ^2 (Stoyan and Stoyan 1994). The critical spatial scale (or cluster size) of the Thomas process is the approximate radius of the clusters, that is, 2σ (see app. A). Note that a cluster in a Thomas process is not necessarily a cluster in a literary sense (i.e., not a local accumulation of points as in, e.g., Plotkin et al. 2002). If the mean number of points per cluster is low, the Thomas process produces empty clusters, that is, clusters that did not receive points or clusters with only one point (fig. 1*B*; app. A). In our example, the expected number of clusters with 0 and 1 point is $68e^{-\mu} = 8.3$ and $68\mu e^{-\mu} = 17.5$, respectively (figs. 1*B*, A1*d*). The pair-correlation function $g(r)$ of the Thomas process yields

$$g(r, \sigma, \rho) = 1 + \frac{1}{\rho}\frac{\exp(-r^2/4\sigma^2)}{4\pi\sigma^2}. \quad (1)$$

The Thomas process thus has three parameters: the intensity λ of the process (which determines the number of points of the pattern; λA), the intensity ρ of the cluster centers, and the parameter σ that determines the cluster size. The unknown parameters (i.e., ρ and σ) can be fitted by comparing the empirical function $\hat{g}(r)$ with the theoretical functions using minimum contrast methods (Stoyan and Stoyan 1994; Diggle 2003; Wiegand et al. 2007*a*).

If different mechanisms that cause clustering act in sequence, the observed spatial pattern may be characterized by small clusters that are nested within large clusters (e.g., Kwit et al. 2007). Conversely, if different mechanisms act independently, large and small clusters (and random patterns) may be independently superposed. The following point processes describe such cases; details on these processes and parameter fitting are provided in appendix A.

2. Double-cluster process: The simple Thomas process (eq. [1]; fig. 1*B*) can be extended to a nested double-cluster process (fig. 1*C*; app. A). In this case, the centers of clusters (with critical spatial scale $2\sigma_2$) are not randomly distributed but are themselves clustered, following a Thomas process (with parameters σ_1 and ρ_1; fig. 1*C*). If $\sigma_1 \gg \sigma_2$, this process shows two easily distinguished critical scales $2\sigma_2$ and $2\sigma_1$. By indicating the parameters ρ and σ of the larger clusters with subscript 1 and those of the smaller clusters with subscript 2, the pair-correlation function of this double-cluster process yields

$$g(r, \sigma_1, \rho_1, \sigma_2, \rho_2) = 1 + \frac{1}{\rho_2}\frac{\exp(-r^2/4\sigma_2^2)}{4\pi\sigma_2^2} + \frac{1}{\rho_1}\frac{\exp(-r^2/4\sigma_{\text{sum}}^2)}{4\pi\sigma_{\text{sum}}^2}, \quad (2)$$

where $\sigma_{\text{sum}}^2 = \sigma_1^2 + \sigma_2^2$ (Wiegand et al. 2007*a*).

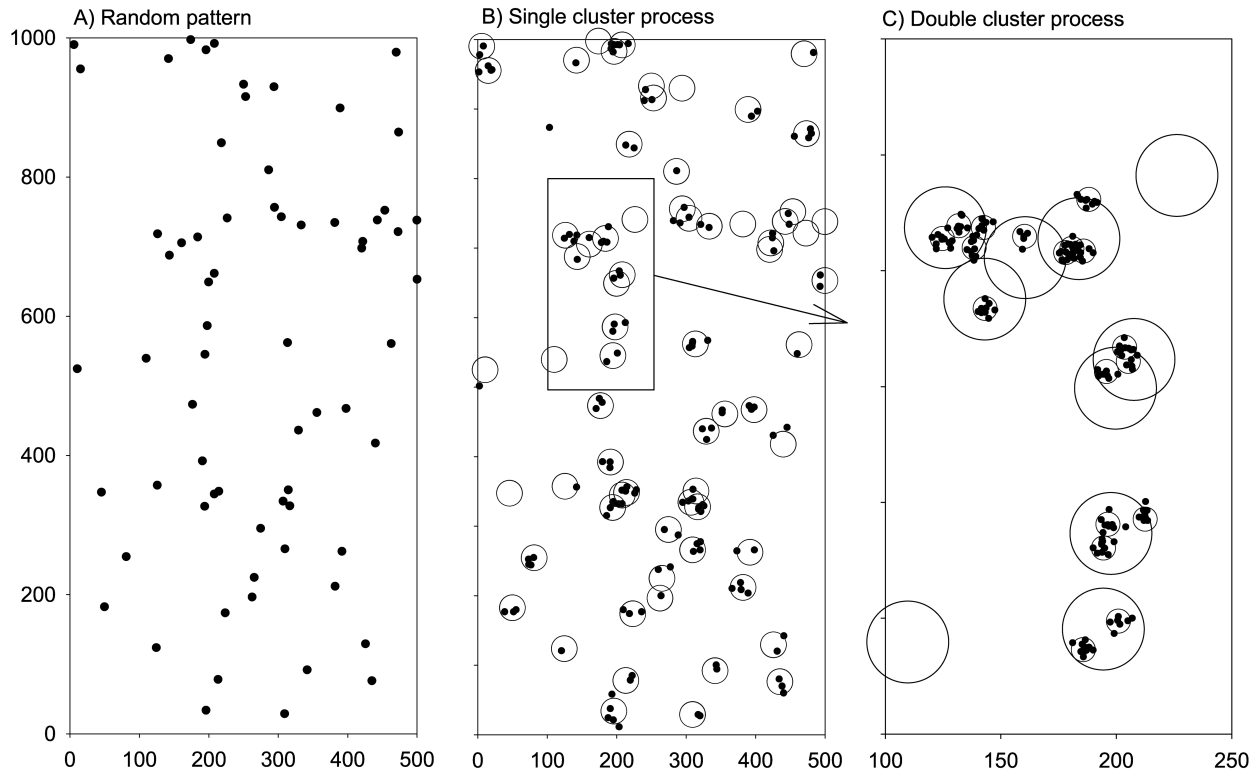

Figure 1: Example of the construction of cluster processes with one and two critical scales of clustering. The first step is a random pattern (*A*); in a second step, the points of the random pattern are replaced by clusters of points yielding a single-cluster Thomas process (*B*); and in a third step, the points of the single cluster process are replaced by clusters of points yielding a nested double-cluster process with two critical scales of clustering (*C*). The random pattern in *A* comprises 68 points, the pattern in *B* comprises 144 points that are randomly distributed over 68 clusters with a cluster size of $2\sigma_1 = 13$ m (*circles*), and the pattern in *C* comprises 1,160 points that are randomly distributed over 144 small clusters with a cluster size $2\sigma_2 = 5.4$ m.

3. Cluster-cluster superposition: Two simple Thomas processes (eq. [1]) may be independently superposed. By denoting the relative intensities of these processes by p_1 and p_2, respectively, and by using the formulas of Illian et al. (2008, p. 371), the pair-correlation function of the superposition process yields

$$g(r, \sigma_1, \rho_1, \sigma_2, \rho_2) = 1 + p_2^2 \frac{1}{\rho_2} \frac{\exp(-r^2/4\sigma_2^2)}{4\pi\sigma_2^2} + p_1^2 \frac{1}{\rho_1} \frac{\exp(-r^2/4\sigma_1^2)}{4\pi\sigma_1^2}, \quad (3)$$

where $p_2^2(1/\rho_2)\{[\exp(-r^2/4\sigma_2^2)]/4\pi\sigma_2^2\}$ is the contribution of Thomas process 2 and $p_1^2(1/\rho_1)\{[\exp(-r^2/4\sigma_1^2)]/4\pi\sigma_1^2\}$ is the contribution of Thomas process 1 (Stoyan and Stoyan 1996; Wiegand et al. 2007*a*). Here the parameters ρ and σ of the two Thomas processes are indicated with subscripts 1 and 2. Comparison of equation (3) with the pair-correlation function of the double-cluster process (eq. [2]) shows that both have the same functional form. However, the estimate of σ_1 will yield a slightly smaller value than σ_{sum} because $\sigma_{\text{sum}}^2 = \sigma_2^2 + \sigma_1^2 > \sigma_1^2$.

4. Double-cluster–random superposition: The pair-correlation function of the independent superposition of a double-cluster process (eq. [2]) and a random pattern yields

$$g(r, \sigma_1, \rho_1, \sigma_2, \rho_2) = 1 + p_C^2 \frac{1}{\rho_2} \frac{\exp(-r^2/4\sigma_2^2)}{4\pi\sigma_2^2} + p_C^2 \frac{1}{\rho_1} \frac{\exp(-r^2/4\sigma_{\text{sum}}^2)}{4\pi\sigma_{\text{sum}}^2}, \quad (4)$$

where $\sigma_{\text{sum}}^2 = \sigma_1^2 + \sigma_2^2$ and where p_C is the proportion of the points belonging to the double-cluster component process (Wiegand et al. 2007*a*). The pair-correlation function of the superposition (eq. [4]) yields exactly the same functional form as that of a double-cluster process (eq. [2]), but a superposition process will have more isolated points

and larger nearest-neighbor distances (see fig. 2*A*, *inset*; fig. 2*D*), which suggests the use of the distribution function $D(y)$ of the nearest-neighbor distances as a criterion to distinguish between both processes. Additionally, the intensity of cluster centers of the double-cluster component process is given by $\rho = \rho^* p_C^2$, where ρ^* is the corresponding estimate for the superposition pattern (Wiegand et al. 2007*a*). The pattern is therefore likely to be a double-cluster–random superposition pattern if $(\rho_1/\rho_1^*)^{0.5} = (\rho_2/\rho_2^*)^{0.5} = p_C$. Note that the properties σ_1, σ_2, and ρ_2/ρ_1 of the double-cluster pattern are not affected by superposition with a random pattern and are therefore more credible characteristics of clustering than are ρ_1 and ρ_2.

Separating a Superposition Pattern

The random component of a double-cluster–random superposition pattern of a given recruitment generation can by separated by identifying isolated recruits that have no neighbors within a certain separation distance. We then joined the resulting component patterns of all five recruitment generations for overall analyses and tested whether the resulting component pattern of isolated recruits was a random pattern (i.e., follow CSR), whether the two component patterns were independent, and whether the second component pattern followed a pure double-cluster process. Additionally, we expect $(\rho_1/\rho_1^*)^{0.5} = (\rho_2/\rho_2^*)^{0.5} = p_C$ (see process 4 above). In practice we tested several decomposition distances to find the one that best satisfied all criteria (for details, see app. A). Note that we cannot expect perfect fits, but the benchmark model should be close to the data to produce credible parameter estimates.

Adult-Recruit Relationships

One natural hypothesis to explain aggregation of recruits is that the clustering is imprinted by the distance to the mother trees and limited dispersal distances. In this case, the recruits of a given generation should be clustered around the reproductive trees from the previous census. Note that this is only a coarse test because, for example, it does not consider the fertility of individual tress (which is important, e.g., in inverse modeling of dispersal kernels; Muller-Landau et al. 2008). To conduct the test, we contrast the bivariate adult-recruit pattern, determined separately for each recruitment generation, with the classical null model of independence (Goreaud and Pélissier 2003). However, to succinctly present our results, we combined the results of the five individual censuses into one average test statistic (see app. C). Following our hypothesis, we included only recruits that belonged to the clustered-component pattern.

Results

Double-Cluster Pattern with Random Component: Cecropia insignis

Although the pair-correlation function of the *C. insignis* recruitment could be fitted well to that of the double-cluster process (eq. [2]; fig. 2*A*), the distribution function $D(y)$ of the distances y to the nearest neighbor clearly shows that the pattern cannot be described by a pure double-cluster process (fig. 2*A*, *inset*). A substantial proportion of recruits had their nearest neighbor at a distance y that was much larger than expected under this null model (i.e., the observed $D(y)$ is substantially below the expected $D(y)$). This suggests that the pattern of recruits is a double-cluster–random superposition. We therefore decomposed the original pattern of each recruitment generation into two components: a cluster-component pattern that contained those recruits that had their nearest neighbor at a distance smaller than a given separation distance (fig. 2*B*), while the rest were contained in the isolated-component pattern (fig. 2*E*). A distance of 8 m yielded the best separation distance.

Indeed, the isolated component was, in good approximation, a random pattern (fig. 2*F*), and both component patterns were independent (fig. 2*F*, *inset*). The double-clustered component pattern yielded a good fit with the pair-correlation function (fig. 2*D*), and the empirical distribution function of distances to the nearest neighbor approximated the expectation under the null model reasonably well (see fig. 2*D*, *inset*; fig. 2*A*). The critical scales of clustering were $r_{C1} = 16.6$ m and $r_{C2} = 5.3$ m, the larger clusters contained on average 17.6 recruits (and 2.1 small clusters), and the small clusters contained on average 8.2 recruits (table 2). For a detailed description of the analysis, see appendix B.

Separate analyses of the pooled 1985, 1990, and 1995 recruits (low recruit numbers did not allow for individual analyses) and the 2000 and 2005 recruitment generations (fig. B1) revealed consistent double-cluster structures among censuses with consistent critical scales (table 2). Recruitment during the 1985–1995 period was relatively low (some 100 recruits per census), but it increased strongly in 2000 and 2005 to 407 and 692 recruits per census, respectively. The proportion of isolated recruits was high during the 1985–1995 periods (31%), but it decreased to 6% and 12% for the 2000 and 2005 censuses, respectively (table 2). The spatial patterns of all subsequent recruitment generations were independent (fig. B2), the clustered component patterns of different periods were independent (fig. B2), and the sum of the estimated numbers of large clusters (26, 14, and 34 for the first, second, and third periods, respectively; table 2) approximated the

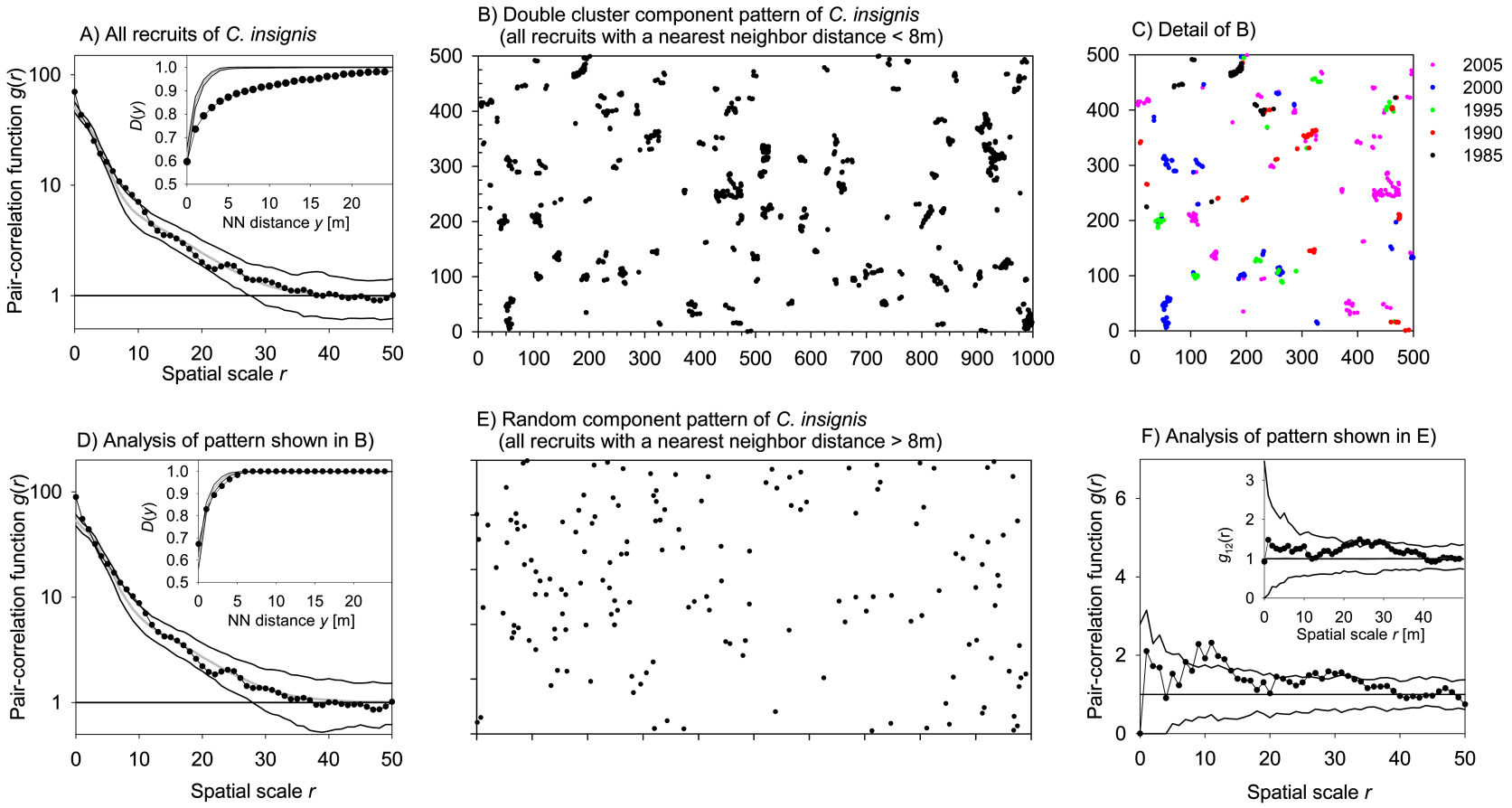

Figure 2: Spatial pattern of all recruits of *Cecropia insignis* during the entire 1985–2005 census period. The pattern is an independent superposition of a random pattern with a double-cluster process. *B*, *E*, Two component patterns of *C. insignis*; *C*, detail of the double-clustered component pattern showing the different recruit generations on the western half of the plot. *A*, *D*, and *F* show the analyses of the pattern of all recruits, the double-clustered component pattern, and the random component pattern, respectively. *A*, Pair-correlation function (*dots*), simulation envelopes (*solid black lines*) indicating the fifth-lowest and -highest values of the pair-correlation function of the 199 simulations of the fitted double-cluster process (eq. [2]), and the fitted double-cluster pair-correlation function (*gray solid line*). The insets in *A* and *D* show the empirical distribution $D(y)$ of the nearest-neighbor (NN) distances y (*dots*), the expected function of the null model (*gray solid line*), and the simulation envelopes (*black solid lines*). *D*, Analogous analysis of the component pattern 1 composed of trees that have a nearest neighbor at a distance $y < 8$ m. *F*, Analysis of component pattern 2 with the complete spatial randomness null model. The inset in *F* shows the test of independence between the two component patterns. Note the logarithmic scale of the *Y*-axis in *A* and *D*. $D(y)$ = cumulative distribution function of the distances y to the nearest neighbor; $g_{12}(r)$ = expected density of trees of type 2 at distance r of an average tree of type 1.

Table 2: Summary of the results of the fit of the recruitment data with the double-cluster process (eq. [2])

							Characteristics of large clusters				Characteristics of small clusters				
Species, component	N	N_{isol}	R_{NN}	p_C	p_{C1}	p_{C2}	$A\rho_1$	σ_{sum}	$2\sigma_1$ (m)	μ_1	$A\rho_2$	$2\sigma_2$ (m)	μ_2	ρ_2/ρ_1	σ_1/σ_2
Figure 1 example:															
Thomas process	144	…	…	1.00	…	…	68	…	17.4	2.1	…	…	…	…	…
Double cluster	1,160	…	…	1.00	…	…	68	9.1	17.4	17.1	144	5.3	8.1	2.1	3.3
Cecropia insignis, all censuses:															
All recruits	1,406	…	…	…	…	…	88	9.0	17.2	15.9	197	5.3	7.1	2.2	3.3
Cluster	1,206	200	8	.9	.88	.86	69	8.7	16.6	17.6	147	5.3	8.2	2.1	3.1
C. insignis, single census:															
1985+1990+1995 cluster	212	95	8	.7	…	…	26	7.4	14.1	8.0	50	4.4	4.3	1.9	3.2
2000 cluster	382	25	8	.9	…	…	14	8.6	16.5	26.7	39	5.1	9.7	2.8	3.2
2005 cluster	612	80	8	.9	…	…	34	8.6	16.3	18.1	78	5.3	7.9	2.3	3.1
Cordia bicolor western, all censuses:															
All recruits	695	…	…	…	…	…	90	10.1	20.0	7.7	920	2.6	.8	10.2	7.6
Cluster	531	164	16	.8	.78	.76	54	10.0	19.9	9.8	531	2.6	1.0	9.8	7.5
C. bicolor western, single census:															
1985 cluster	80	31	16	.7	…	…	20	5.3	10.6	3.9	None	None	…	…	…
Cluster 1990	309	34	16	.90	…	…	44	8.7	17.2	7.1	336	2.4	.9	7.7	7.3
1995+2000+2005 cluster	151	90	16	.6	…	…	36	7.7	15.1	4.2	267	2.6	.6	7.4	5.8
C. bicolor eastern, all censuses:															
All recruits	209	…	…	…	…	…	69	10.8	21.5	3.0	283	2.7	.7	4.1	7.9
Cluster	113	96	16	.5	.61	.53	26	10.0	19.8	4.4	80	2.8	1.4	3.1	7.1
C. bicolor, entire plot:															
1995+2000+2005 cluster	193	150	16	.6	…	…	50	7.8	15.5	3.9	346	2.5	.6	7.0	6.1
Miconia argentea, all censuses:															
All recruits	1,666	…	…	…	…	…	309	6.3	12.2	5.4	977	3.0	1.71	3.2	4.1
Cluster	1,331	335	12	.80	.78	.90	186	6.3	12.3	7.2	784	2.7	1.70	4.2	4.6
M. argentea, single census:															
1985 cluster	232	56	12	.8	…	…	45	7.3	14.4	5.2	104	2.8	2.23	2.3	5.1
1990 cluster	416	101	12	.80	…	…	57	7.7	15.1	7.3	292	2.6	1.42	5.1	5.9
1995 cluster	299	52	12	.9	…	…	41	5.1	9.9	7.4	258	2.2	1.16	6.4	4.5
2000 cluster	190	55	12	.8	…	…	33	5.4	10.4	5.8	84	2.7	2.26	2.6	3.9
2005 cluster	194	71	12	.7	…	…	48	6.8	13.3	4.0	215	2.9	.90	4.5	4.6
Randia armata, all censuses:	340	0	…	1.00	…	…	129	27.8	55.5	2.6	2,395.8	3.5	.14	18.5	16.0
Hasseltia floribunda, all censuses:	147	0	…	1.00	…	…	137	10.0	19.8	1.1	571	3.0	.26	4.2	6.7

Note: N = total number of recruits; N_{isol} = number of recruits in isolated component pattern; R_{NN} = decomposition distance used to separate the clustered and the isolated component patterns (NN = nearest neighbor); p_C = proportion of recruits in isolated component pattern; p_{C1}, p_{C2} = predicted values of p_C based on the fitted parameters ρ of the large and small clusters, respectively; ρ_1, σ_{sum} = fittest parameters of large clusters; ρ_2, σ_2 = fittest parameters of the small clusters; μ_1, μ_2 = average number of trees in one large-scale and one small-scale cluster, respectively; and ρ_2/ρ_1 = average number of small clusters in one large cluster.

number of clusters of the joined clustered component pattern well (69; table 2).

Cordia bicolor

The spatial pattern of recruits of the species *C. bicolor* showed a heterogeneous pattern (fig. 3*B*), with a higher density at the western part of the plot. This part of the plot is dominated by a low plateau habitat, and the eastern subplot contains a high plateau and slope habitats (Harms et al. 2001). Small trees of *C. bicolor* show a weak positive association with the low plateau ($P = .0512$; Comita et al. 2007*a*). However, the patterns were approximately homogeneous within each subplot (fig. 3*B*). We therefore analyzed the western and eastern parts of the study plot separately.

We found that the patterns of the two subplots were, in good approximation, independent superpositions of a double-clustered and a random pattern. Despite the heterogeneous appearance of the accumulated recruitment patterns (fig. 3*B*, 3*E*), the two subplots showed striking structural similarities. First, the critical scales of the double-cluster processes (i.e., 20 and 2.8 m) were the same for the two subplots (table 2). Second, the average number of recruits per small cluster was low (i.e., $\mu_2 = 1.0$ and

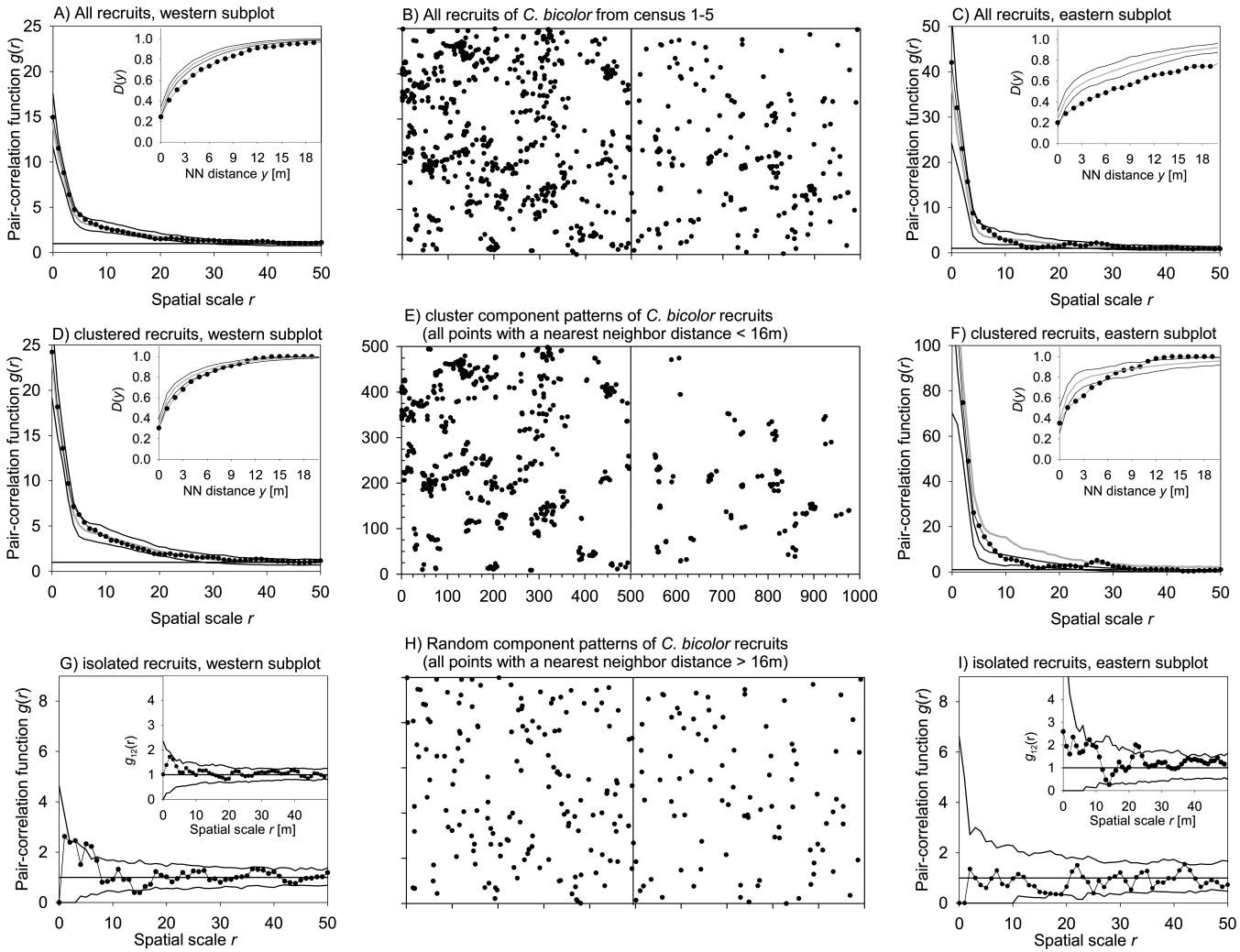

Figure 3: Analysis of the spatial pattern of *Cordia bicolor*. Because of heterogeneity of the pattern, we analyzed the approximately homogeneous western and eastern parts of the study plot separately. The pattern of *C. bicolor* was a superposition pattern of a double-clustered component pattern (*E*) and a random component pattern (*H*). *A*, *C*, Analysis of recruitment pattern from the two parts of the study plot. *D*, *F*, Analysis of double-clustered component patterns from the two parts of the study plot. *G*, *I*, Analysis of component pattern 2 from the two parts of the study plot with the complete spatial randomness null model. The insets show the test of independence between the two corresponding component patterns. Other conventions are as they are in figure 2.

1.4 for the western and the eastern subplot, respectively; table 2), and not all recruits had a neighbor within the same small cluster (the Poisson distribution predicts that only 41% and 54% of all *C. bicolor* recruits of the western and the eastern subplot, respectively, had at least one neighbor within the small cluster). However, this occasional pairing of recruits imprinted a strong signal at the pair-correlation function (i.e., a steep decrease in $g(r)$ from scale $r = 1$ m to scale $r = 5$ m; fig. 3*A*, 3*C*, 3*D*, 3*F*). Third, the random component patterns from the two subplots formed one (homogeneous) random pattern (fig. 3*H*). However, the average number of recruits per large cluster (μ_1) was two times larger at the western subplot than at the eastern subplot (table 2). For details, see appendix B.

Analysis of the temporal dynamics of the recruitment patterns revealed interesting additional insights. First, the number of isolated recruits was relatively constant, yielding an average ± SD of 31 ± 9 recruits at the western subplot and 19.2 ± 3.4 recruits at the eastern subplot. However, the number of recruits assigned to the clustered component patterns showed a marked peak in the 1990 census, yielding more than four times more recruits than in the other census periods. Second, the temporal evolution of the clustered component pattern of the 1985 and the 1990 censuses and the pooled data of the 1995, 2000, and 2005 census periods suggest an invasion process at the eastern subplot (fig. B3). While the 1985 census data showed only a few *C. bicolor* clusters (fig. B3*a*), recruit clusters had already invaded most of the eastern plot in the 1990 census (fig. B3*c*). Finally, at the 1995+2000+2005 census, both the cluster component and the isolated component yielded a homogeneous pattern over the entire 50-ha plot (fig. B3*e*, B3*g*). The cluster component of the 1995+2000+2005 census could be fitted well with a double-cluster process (fig. B3*f*), the isolated component was a random pattern (fig. B3*h*), and the two component patterns were independent (fig. B3*h*, *inset*).

Analysis of the cluster-component patterns of the western subplot showed that the patterns of recruits of the 1985 and 1990 (and the 1995 and 2000+2005) censuses were independent; however, those of the 1990 and 1995 censuses were not, and these showed strong attractions especially at spatial scales <5 m (fig. B4).

Double-Cluster Pattern with Random Component: Miconia argentea

The spatial pattern of *M. argentea* can be decomposed into a double-clustered component pattern (fig. 4*B*, 4*D*) and a random component pattern (fig. 4*E*, 4*F*), although the two component patterns are not fully independent (fig. 4*F*, *inset*). The double-clustered component pattern yielded a good fit with the pair-correlation function at smaller scales (fig. 4*D*). We observed departure from the null model at scales of 20–35 m, which is due to some large clusters in the area of the swamp and the stream in the western part of the plot (fig. 4*B*). (Large *M. argentea* trees showed a weak association with the swamp habitat; Comita et al. 2007*a*.) The critical scales of clustering were $r_{C1} = 12.3$ m and $r_{C2} = 2.7$ m, the larger clusters contained 7.2 recruits (and 4.2 small clusters) on average, and the small clusters contained 1.7 recruits (table 2).

Separate analyses of the different recruitment generations revealed consistent double-cluster structures among censuses, with critical scales ranging between 10–15 m and 2.2–2.9 m (table 2). The average number of small clusters within large clusters ranged between 2.3 and 6.4 (table 2). Interestingly, the spatial patterns of all subsequent recruitment generations were spatially dependent at scales <10 m (fig. B6), but recruitment generations that were 10 years apart were independent. Consequently, the sum of the estimates of the number of large-scale and small-scale clusters of individual censuses was larger than the corresponding estimates of all censuses together (186 vs. 234 and 784 vs. 953; table 2). This points to an overlap in clusters among generations. Thus, *M. argentea* showed regeneration hotspots (Hampe et al. 2008) that consistently persisted from one into the next recruitment generation (but not longer).

Pure Double-Cluster Pattern: Hasseltia floribunda

The large trees of the species *H. floribunda* showed some weak negative habitat association to the high plateau and a positive association to the small areas of swamp and streamside (Harms et al. 2001). This habitat association, however, did not translate into heterogeneity of the recruit pattern; the pair-correlation function dropped for larger scales to values of 1 (fig. 5*A*). The recruits showed a double-cluster pattern, with critical scales of clustering of 20 m and 3 m (fig. 5*A*; table 2) but without superposition of a random component pattern. The pair-correlation function of the data was in good agreement with the double-cluster model (fig. 5*A*). However, the distribution function of the distances to the nearest neighbor showed minor differences at nearest neighbor distances >20 m (fig. 5*A*, *inset*). The average number of recruits per small cluster was low, with $\mu_2 = 0.26$ (table 2). Application of a Poisson distribution with mean $\mu_2 = 0.26$ predicts that 88% of all *H. floribunda* recruits occurred alone, 11% were in pairs, and 1% were in groups of three. This small-scale grouping left a clear signature at the pair-correlation function (i.e., a steep decrease from scales $r = 1$ m to $r = 6$ m; fig. 5*A*).

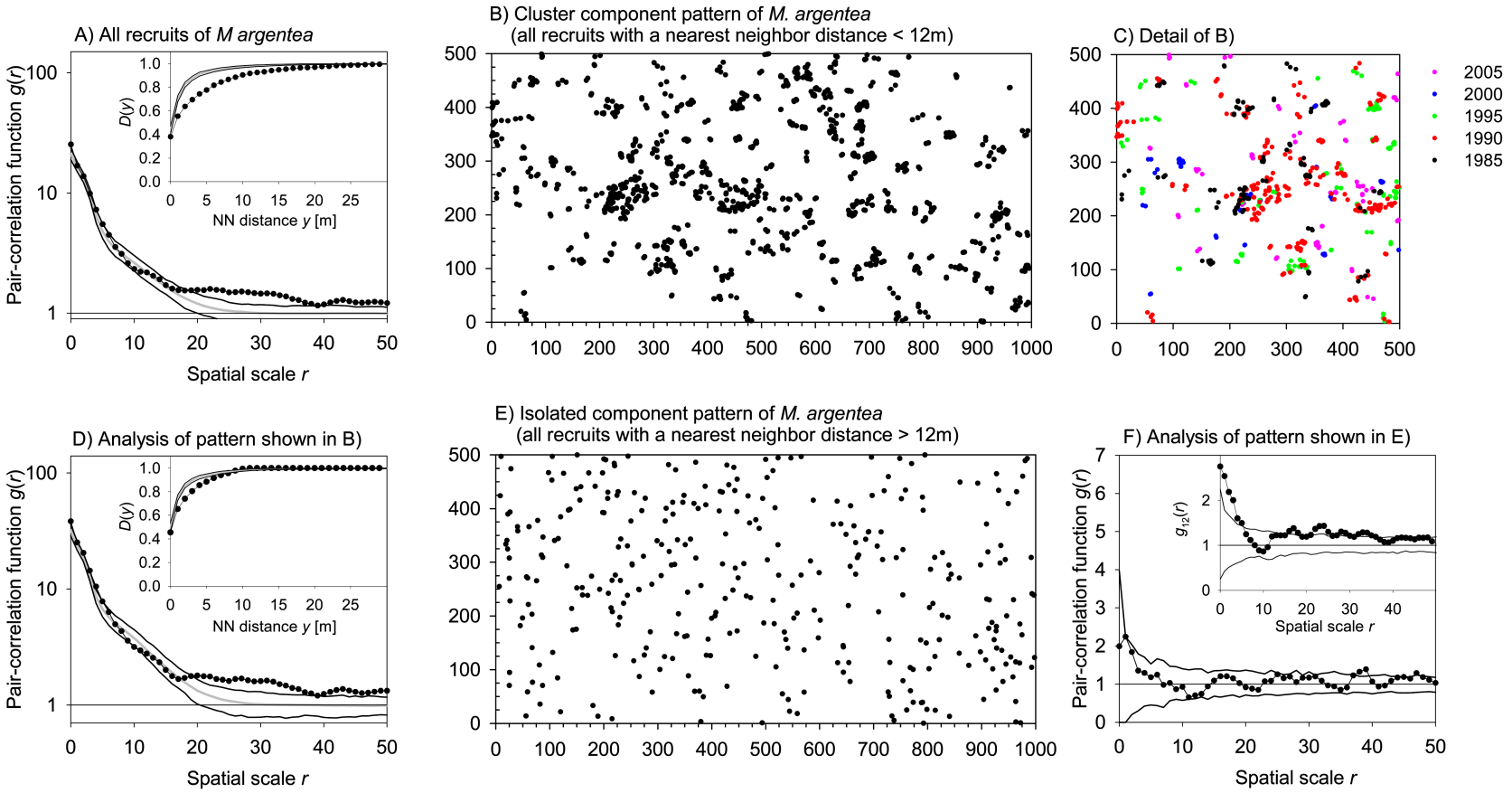

Figure 4: Analysis of the spatial pattern of *Miconia argentea*. *A*, *D*, Analyses of the patterns of all recruits and of the double-clustered pattern shown in *B*, respectively. *C*, Detail of the double-clustered component showing regeneration hotspots. *F*, Analysis of the random component pattern shown in *E*. Other conventions are as they are in figure 2.

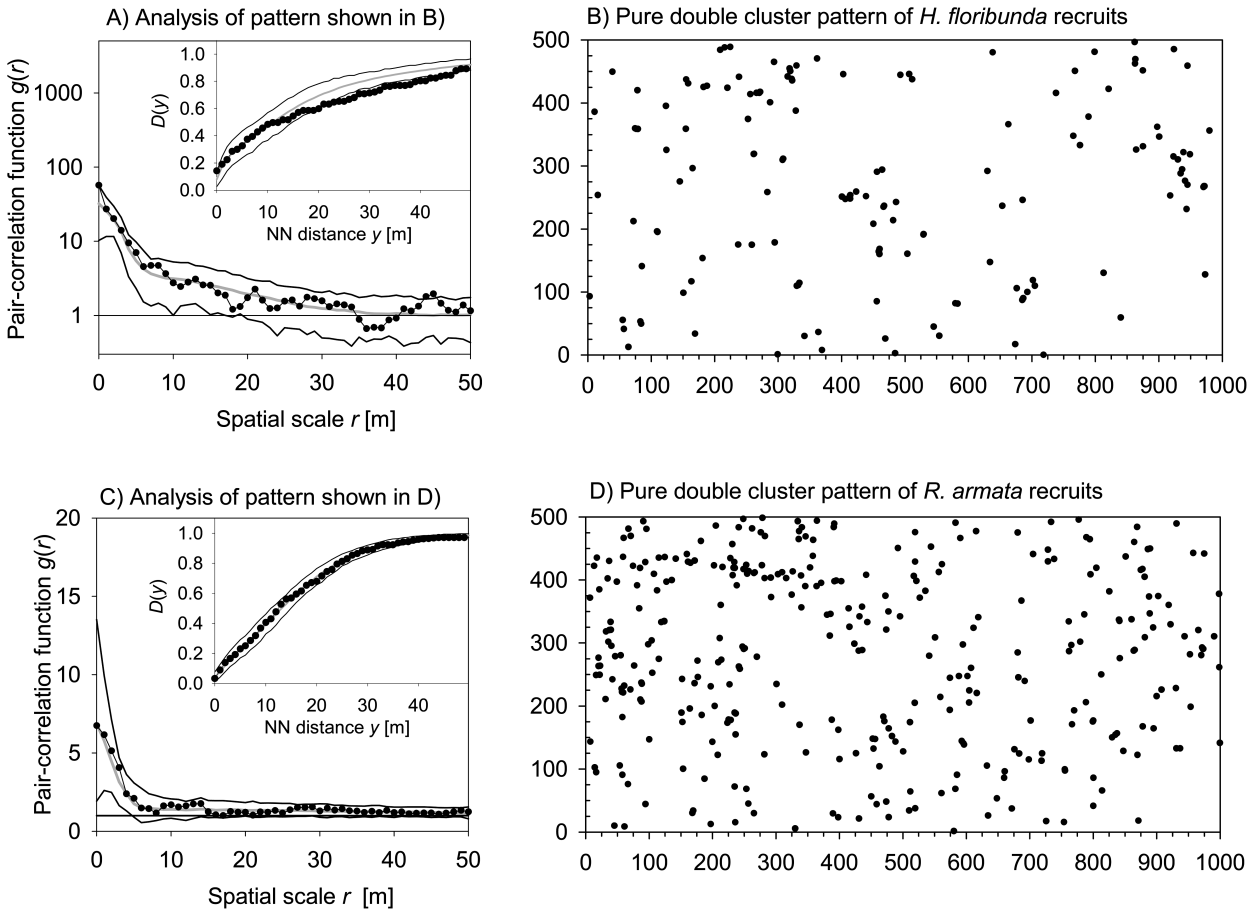

Figure 5: Analysis of spatial patterns of *Hasseltia floribunda* (*A*, *B*) and *Randia armata* (*C*, *D*). Conventions are as they are in figure 2. Note the logarithmic scale of the *Y*-axis in *A*.

Pure Double-Cluster Pattern: Randia armata

The spatial pattern of recruits of *R. armata* could be fitted well to a double-cluster process with critical scales of clustering of 56 m and 3.5 m (fig. 5*C*; table 2), but no superposition pattern could be detected. The mean number of recruits per large and small cluster yielded $\mu_1 = 2.6$ and $\mu_2 = 0.14$, respectively (table 2). Thus, 93% of all *H. floribunda* recruits are predicted to occur alone, and 7% are predicted to occur in pairs. The 7% that were grouped recruits left a detectable signal of small-scale clustering in the pair-correlation function.

Adult-Recruit Relationships

Our analysis revealed a tendency toward repulsion between recruits and reproductive trees of *C. insignis* (fig. B7*a*) and independence for *C. bicolor* (at the western subplot; fig. B7*b*) and for *R. armata* (fig. B7*e*). However, recruits of the species *H. floribunda* were clearly "attracted" by reproductive trees at distances up to 10 m, which coincides with the critical scale of larger-scale clustering (fig. B7*c*). Recruits of the clustered-component pattern of *M. argentea* were positively associated with reproductive trees at distances >20 m (fig. B7*d*).

Relationship Between Model Parameters and Species Traits

An expected geometric relationship is that the number of small clusters that fit into large clusters (with respect to area; i.e., $\pi\sigma_1^2/\pi\sigma_2^2$) should be positively correlated with the average number of small clusters within large clusters (i.e., ρ_2/ρ_1). Indeed, the Spearman rank correlation yielded $r_{Sp} = 0.8$ ($P < .01$; table D1). We found several highly significant correlations between species characteristics and cluster model parameters (table D1). The species property that most strongly correlated with cluster properties was the coefficient b characterizing the light sensitivity of recruits

(Rüger et al. 2009). The higher the light sensitivity, the larger the mean number of recruits in small and large clusters (b vs. μ_1: $r_{Sp} = -0.88$, $P < .01$; b vs. μ_2: $r_{Sp} = -0.94$, $P < .01$). Additionally, the more light-sensitive the recruits, the smaller the size of the small clusters relative to the size of the large clusters (b vs. σ_1/σ_2: $r_{Sp} = -0.93$, $P < .01$). The same tendencies were found for the seed weight and the maximal sapling growth rate (an indicator of a species' shade tolerance; Comita et al. 2007*a*), but these were somewhat weaker (table D1). A crude measure of dispersal quantity by *Cebus* monkeys (*eff*; table D1) was positively correlated with the light coefficient b. Interestingly, the proportion p_C of recruits that belong to the random component pattern was not strongly correlated with any species property.

Discussion

In this article we provide methods of spatial statistics that can help to discern mechanisms involved in the (animal) dispersal of plant seeds from analysis of the spatial pattern of recruits. This is an important issue because, in tropical forests for example, up to 90% of trees and understory shrubs have fleshy fruits that attract animals as seed dispersers (e.g., Howe and Smallwood 1982; Muller-Landau and Hardesty 2005). Consequently, linking dispersal mechanisms with the spatial processes that they generate and with the observed spatial patterns of plants that recruit to a particular life stage is one of the large challenges of seed dispersal biology (Clark et al. 1999*a*; Nathan and Muller-Landau 2000). Because seed dispersal in nature is difficult to quantify directly for plants and especially for forest trees, inverse models (Ribbens et al. 1994; Clark et al. 1999*b*) and mechanistic models (Russo et al. 2006; Carlo and Morales 2008; Levey et al. 2008) have played a prominent role in predicting the spatial distributions of seeds (Muller-Landau and Hardesty 2005; Russo et al. 2006). Inverse modeling techniques based on seed dispersal kernels are descriptive techniques that have difficulties in accounting for overlapping seed shadows caused by different dispersal agents (Dennis and Westcott 2007) and describing spatially aggregated seed-deposition patterns. However, if seed dispersal models do not consider clumping of seeds, biased estimates of seedling population dynamics will result (Chesson et al. 2005).

Our method focuses on a detailed description of the spatial patterns. We analyzed the spatial patterns of recruits at the BCI tropical forest and found marked, clearly identifiable spatial structures that were temporally consistent. This is an important result that shows that our techniques allow for the extraction of detailed information from the patterns (i.e., uncertainty in the fitted parameters is moderate or small). More importantly, the temporal consistency of the spatial structures strongly suggests that biological organization exists and that the link between process and pattern could be uncovered (McIntire and Fajardo 2009). A close description of the characteristics of the observed spatial patterns (e.g., critical scales of clustering, relative proportions of scattered vs. clustered recruits, temporal consistency of spatial patterns) may allow for deriving hypotheses and inferences about the underlying spatial processes. However, additional data on species properties are necessary to correctly interpret the patterns in terms of the processes.

Finally, implementing and testing these hypotheses as approaches of forward prediction of spatial patterns that are based on directly modeling the behavior of the seed dispersal agents such as wind, primates, or birds (e.g., Russo et al. 2006; Carlo and Morales 2008; Levey et al. 2008) are some of the most important next steps for dispersal biology. The spatial analysis techniques presented here can serve for both in this respect, in designing models and testing the reliability of the predicted patterns (i.e., to determine whether the model produces patterns that resemble the observed patterns; Wiegand et al. 2003; Grimm et al. 2005).

Gains of Our Approach

Our approach allows for an extraction of information from spatial patterns that has previously not been possible. Our analyses revealed the existence of surprising spatial structures such as the double-cluster and superposition patterns. All five study species showed clustering at (at least) two critical spatial scales, and three species showed an independent superposition pattern of a double-cluster pattern with a random pattern. When we first detected such complex spatial patterns for a tropical tree species in Sri Lanka, we suspected that they might be rare (Wiegand et al. 2007*a*). However, our current analysis suggests that double-cluster and superposition patterns may be more common than previously thought but were not detected because appropriate methods to do so were not available. Many different spatial processes and mechanisms such as gap structures, soil nutrients, dispersal limitation, or secondary seed dispersal by animals are known to create clustered spatial patterns in tropical forests (e.g., He et al. 1997; Hubbell et al. 1999; Plotkin et al. 2000; Svenning et al. 2006) and other plant communities (Purves and Law 2002; Getzin et al. 2008). There is no reason to assume that all should show the same critical spatial scale (Wiegand et al. 2007*a*). Multiple cluster processes should therefore be a common phenomenon. What is indeed more surprising is the existence of clear superposition patterns, as was found here for the three pioneer species.

The superposition patterns detected here have consequences for estimates of seed dispersal kernels. We found that the recruitment of the pioneer species we analyzed

comprised two independent populations: one in which recruits appear in groups and one resulting in a random pattern within the study plot. It is somewhat unlikely that such a pattern would be caused by (fine-scale) environmental conditions (especially regarding the specific invasion case of *Cordia bicolor*). It is more likely that this phenomenon is caused by two different seed dispersal modes: one scatter-dispersal mode and one clump-dispersal mode (Howe 1989). This means that our pattern analysis techniques are able to determine the relative importance of scatter dispersal for effective seed dispersal (i.e., seeds that survived at least until the recruit stage) on only the basis of the information about recruits, without direct field measurements of seed dispersal. This surprising result demonstrates the high potential of refined spatial pattern analysis techniques. In one case (*Cecropia insignis*), our result contrasted sharply with previous inferences from inverse modeling. We found that the random component pattern comprised, on average, 14% of all recruits, but estimates of seed dispersal kernels based on seed trap data suggested a strong dispersal limitation for this species (the estimated a median dispersal distance was 0.8 m; Dalling et al. 2002). Note that *C. insignis* is a difficult species to detect, with very small seeds that may pass through the mesh traps or that may otherwise go undetected (Dalling et al. 2002). Our methodology is thus a valuable method to complement the limitations of the traditional analyses of seed dispersal kernels. However, an alternative hypothesis would be that isolated recruits appear in randomly spaced small canopy gaps.

In general, the spatial structures revealed by our analyses were temporally consistent. The constancy in the structural properties of the three pioneer species suggest that the cluster component patterns may be imprinted by animals with a particular behavior (e.g., scatter dispersal vs. clump dispersal), probably in combination with local conditions such as light climate within canopy gaps (deciding germination and survival and shaping the cluster sizes). However, the numbers of clusters (and recruits) varied somewhat among years, probably as a consequence of interannual variations in fecundity. The cluster component of the recruit populations of *C. insignis* comprised randomly distributed clusters that were also independent among censuses. This is consistent with the large growth rate of *C. insignis* (table 1) and its short-lived seed bank, wherein most seeds survive <1 year (Gallery et al. 2007). However, although the species *Miconia argentea* showed temporally consistent double-cluster structures, the clusters were not independent between subsequent censuses, pointing to certain regeneration hotspots (Hampe et al. 2008) that persisted from one recruitment generation into the next. These hotspots might be related to a positive association of recruits at distances of 20–40 m away from reproductive trees (fig. B7), which is in accordance with large dispersal distances (with a median distance of 51.5 m; Dalling et al. 2002). However, these hotspots might also be mediated by the positive association of trees of this species to the swamp habitat (Harms et al. 2001; Comita et al. 2007*a*) or related to the somewhat lower growth rate, which was the smallest among the pioneer species (table 1). The spatial patterns of subsequent *C. bicolor* recruitment generations showed spatial attraction for only the 1990 and 1995 censuses. One reason for this may be that the census artificially divided one actual recruitment generation into two; note that the 1990 census showed an unusual peak in recruitment.

We found indications for only one species (*Hasseltia floribunda*) that the critical scales of clustering were related to the position of reproductive trees. This suggests that the seed shadows of many species may be considerably modified during the transitions to recruits, for example, by mortality due to insufficient light or Janzen-Connell effects (Janzen 1970; Connell 1971). For *C. insignis*, we observed small-scale repulsion between reproductive trees and recruits that points to Janzen-Connell effects. Correlations of cluster characteristics and measures of shade tolerance suggest that species-specific interactions between the local light climate and shade tolerance may be additionally involved in generating the observed cluster structures. For example, recruits of light-demanding species group together more than do recruits of shade-tolerant species, and the more light-demanding the recruits, the smaller the size of the small clusters relative to the size of the large clusters. A crude measure of dispersal quantity by *Cebus* monkeys was strongly correlated with the measures of shade tolerance, which precludes stronger statements on the role of *Cebus* in generating the observed patterns. However, our results clearly show that biological organization exists, and we are confident that analyzing more species with the methods presented here will allow for stronger statements.

Conclusions

Our analyses revealed the existence of surprising spatial structures, such as double-cluster and superposition patterns, and our results suggest that these structures may be much more common phenomena (at least for tropical tree species) than previously thought. These are considerable gains, but it has to be noted that these findings required more complex null models than are usually used in ecology to describe the complex structures found in ecosystems. Our findings clearly suggest that biological organization exists, but the observed spatial recruitment patterns cannot be attributed to a universal mechanism but rather to idiosyncratic interactions among several mechanisms such

as animal dispersal (creating clumped and scatter seed depositions), local light climate and regeneration hotspots, and dispersal limitation (shaping the critical scales of clustering). An important challenge of future research is to disentangle these mechanisms by conducting analyses of the type presented here, but for a large number of species, and to systematically relate species traits to characteristics of the observed spatial patterns. We are just beginning to discover the richness of spatial patterns found in tropical forests, and we are confident that a combination of advanced point pattern analysis with field data will allow for significant advances in establishing the link between spatial patterns and processes.

Acknowledgments

The Barro Colorado Island forest dynamics research project was made possible by National Science Foundation grants to S. P. Hubbell. (DEB-0640386, DEB-0425651, DEB-0346488, DEB-0129874, DEB-00753102, DEB-9909347, DEB-9615226, DEB-9615226, DEB-9405933, DEB-9221033, DEB-9100058, DEB-8906869, DEB-8605042, DEB-8206992, and DEB-7922197); by support from the Center for Tropical Forest Science, the Smithsonian Tropical Research Institute, the John D. and Catherine T. MacArthur Foundation, the Mellon Foundation, the Celera Foundation, and numerous private individuals; and through the hard work of over 100 people from 10 countries over the past two decades. The plot project is part the Center for Tropical Forest Science, a global network of large-scale demographic tree plots. The manuscript benefited from discussions with N. Rüger and R. Condit, and two anonymous reviewers provided constructive comments on earlier drafts of the manuscript. T.W. was supported by a European Research Council (ERC) advanced grant (233066).

APPENDIX A

Cluster Processes

Single-Cluster Process (Thomas Process)

The Thomas process (Thomas 1949) is an algorithm that produces relatively realistic clustered point patterns based on a simple stochastic construction principle. It has the big advantage that its pair-correlation function and the distribution function of the nearest neighbor distances can be calculated analytically (Stoyan and Stoyan 1994). This allows one to fit the Thomas process to given point pattern data with standard tools. Consequently, the Thomas process has been applied to tropical tree species in several studies (e.g., Plotkin et al. 2000; Seidler and Plotkin 2006; Wiegand et al. 2007*a*). However, note that the Thomas process is phenomenological, not mechanistic, and it does not provide a direct link to the underlying processes, although the parameter σ reflecting the size of clusters has been found to correlate with the dispersal capacity of tropical tree species (Seidler and Plotkin 2006). Here we used the Thomas cluster process and other more complex cluster processes that are based on the Thomas process as benchmark processes with known structures for measuring basic properties of the aggregation structures of the patterns of recruits (Wiegand et al. 2007*a*). This is a prerequisite for deriving specific hypotheses about the underlying processes. Note that the fitted parameters of the cluster processes allowed us to simulate point patterns with spatial structures similar to the observed point pattern.

The construction principle of the Thomas process is simple: a certain number of clusters are randomly and independently distributed over a given study region with area A (see fig. A1*a*). The pattern shown in the example comprises 68 clusters (fig. A1*a*, *gray disks*). The positions of the cluster centers (fig. A1*a*, *dots*) follow a homogeneous Poisson process with intensity $\rho = 68/(1{,}000\text{ m} \times 500\text{ m}) = 1.36\text{ ha}^{-1}$ (fig. A1*b*).

When the coordinates of the cluster centers are determined, the individual clusters are constructed. To this end, the points of the pattern (the pattern shown in fig. A1*c*, which comprises $\lambda A = 144$ points) are randomly assigned to the clusters. Thus, the number of points that belong to a given cluster follow a Poisson distribution with mean $\mu = \lambda/\rho = 144/68 = 2.1$. Note that this also means that a given cluster may be empty (i.e., there is no point assigned to the cluster); the probability of a given cluster being empty is $P[n = 0, \mu] = \exp(-\mu)$, and the probability of having just one point is $P[n = 1, \mu] = \mu \exp(-\mu)$. In the example, 11 clusters were empty clusters, 14 clusters received one point, 18 clusters received two points, and the maximal observed number of points per cluster was six (fig. A1*d*, *inset*). It is important to keep this construction principle in mind when interpreting the parameters that were fitted to a given data set using a Thomas process.

The second part of the construction of the clusters is the determination of the locations of the points that belong to a given cluster: the locations of the points in a given cluster relative to the cluster center follow a bivariate Gaussian

distribution $h(r, \sigma)$ with variance σ^2. Note that other distribution functions are also possible. For example, in a Matern process, the points of a given cluster are randomly placed within a disk of radius R around the cluster center (Stoyan and Stoyan 1994). However, the distribution used in the Thomas process results in a simpler equation for the pair-correlation function, which makes it more suitable as a construction unit for more complex double-cluster processes. It is also biologically more plausible that the density of points within a cluster declines with increasing distance from the cluster center.

The Thomas process has three parameters: the intensity λ of the process (which determines the number of points of the pattern; λA), the intensity ρ of the cluster centers, and the parameter σ that determines the cluster size. The pair-correlation function $g(r)$ of the Thomas process yields

$$g(r, \sigma, \rho) = 1 + \frac{1}{\rho} \frac{\exp(-r^2/4\sigma^2)}{4\pi\sigma^2}. \tag{A1}$$

If the number of clusters (ρA) decreases (under a fixed number of points), the degree of clustering of the pattern increases because the points are now concentrated in fewer clusters. The degree of clustering will also increase if the variance σ of the normal distribution (which determines the location of the points relative to the cluster center) decreases, because the points are now closer together. The distance $r_C = 2\sigma$ from the cluster centers, within which 86% of all points are located, can be used to describe the typical size of the clusters of the Thomas process. In the example, the cluster size is 17.4 m. The approximate area covered by a given cluster is thus given by $A_C = \pi r_C^2 = 4\pi\sigma^2$. Because formally distinct clusters may coalesce, it is difficult to identify the points that belong to a given cluster with any confidence (fig. A1*c*). Note that this definition of a cluster size is not directly related to properties of individual clusters (e.g., the number of points belonging to a given cluster; e.g., Plotkin et al. 2002) but is based on the (stochastic) construction principle of the clusters. If the average number of points per cluster is high (say, $\mu > 3$; see fig. A2), most of the clusters have more than one point and could be named clusters in a literary sense. Thus, care has to be taken to not interpret the fitted parameters too literally (i.e., search clearly visible clusters with radius $r_C = 2\sigma$) if the mean number $\mu = \lambda/\rho$ of points per cluster is low (fig. A2).

"Empty clusters," or clusters with only one or two points, may frequently occur, especially if the number of points of the process is relatively low. However, even if the total number of points of the process is relatively high, a given cluster pattern may be characterized by $\rho \gg \lambda$; that is, there are more clusters than points in the process. Although this is somewhat counterintuitive on the first viewing (with a descriptive definition of clusters in mind), it makes perfect sense and describes a situation where most points are isolated points but where occasionally two or three points are paired close together. This is an important class of cluster processes that is well covered by the Thomas process. For example, if the mean number of points per cluster is $\mu = 0.25$, the Poisson distribution predicts that 78% are empty clusters, 19% are clusters with one point, and 3% are clusters with more than one point. With this constellation, 78% of all points of the Thomas process are isolated points (i.e., belonging to clusters with only one point), 19% of all points have one nearby neighbor (i.e., they belong to clusters with two points), and 3% belong to clusters with three or more points.

The pair-correlation function at $r = 0$ is related to the probability that a given point of the pattern has a neighbor very close by. This is a useful characteristic of the Thomas process that describes the overall degree of clustering. It yields

$$g(r = 0, \sigma, \rho) = 1 + \frac{1}{\rho} \frac{1}{4\pi\sigma^2} = 1 + \frac{1}{\rho} \frac{1}{A_C}. \tag{A2}$$

Thus, both the area of the cluster and the number of clusters determine the overall clustering in the same way. This reflects the intuitive fact that the degree of clustering may increase if there are fewer clusters or if the area covered by individual clusters is smaller. However, the decline of the pair-correlation function with scale r depends on only the cluster size A_C:

$$g(r, \sigma, \rho) = 1 + \frac{1}{\rho A_C} \exp\left(-\frac{\pi r^2}{A_C}\right), \tag{A3}$$

with a rate of decline that is given by the relative area of the disk with radius r measured in units of the cluster size A_C.

Double-Cluster Process

The simple Thomas process described in the last section can be extended to a double-cluster process. In this case, the cluster centers are themselves clustered and follow a Thomas process (fig. A1*e*). Note that this nested construction principle is the same as it is for a Thomas process, where the cluster centers follow a complete spatial randomness (CSR) process (also called a multigeneration process; Diggle 2003). Thus, small clusters are located within larger clusters (fig. A1*e*). In the example, there are 1,160 points distributed over 144 small clusters with size $r_C = 5.3$ m; thus, there are, on average, $\mu = \lambda/\rho = 8.06$ points within one small cluster, and small clusters with only a few points are rare (fig. A1*f*, *inset*; table 2).

The double-cluster process has five parameters: the intensity λ of the process (which determines the number of points of the pattern; λA), two parameters σ that describe the size of the clusters, and two parameters ρ that describe the number of clusters. By indicating the parameters of the larger clusters with subscript 1 and those of the smaller clusters with subscript 2, the pair-correlation function of this double-clustered process yields

$$g(r, \sigma_1, \rho_1, \sigma_2, \rho_2) = 1 + \frac{1}{\rho_2}\frac{\exp(-r^2/4\sigma_2^2)}{4\pi\sigma_2^2} + \frac{1}{\rho_1}\frac{\exp(-r^2/4\sigma_{\text{sum}}^2)}{4\pi\sigma_{\text{sum}}^2}, \tag{A4}$$

where $\sigma_{\text{sum}}^2 = \sigma_1^2 + \sigma_2^2$ (Wiegand et al. 2007*a*). Clearly, the two scales of clustering can only be separated if small clusters are distributed within large clusters, that is, $\sigma_1 \gg \sigma_2$. This is the case in our example, where $\sigma_1 = 8.69$ and $\sigma_2 = 2.64$. On the other hand, if large clusters were distributed within small clusters (i.e., $\sigma_1 \ll \sigma_2$), then $\sigma_{\text{sum}} \approx \sigma_2$ and equation (A4) approximates the pair-correlation function of the simple Thomas process (eq. [A1]) with intensity $1/\rho = (1/\rho_2 + 1/\rho_1)$. If the centers of the small clusters are not clustered (i.e., $\sigma_2 \to \infty$), equation (A4) collapses to equation (A1), because in this case the process is a simple Thomas process.

Parameter Fitting

For parameter fitting, we followed the minimal-contrast method described, for example, in Stoyan and Stoyan (1994) and in Diggle (2003). However, as suggested in Wiegand et al. (2007*a*), we fitted both the g function and the L function simultaneously. Theoretically, the g and L functions contain the same information, and fitting using g or L should therefore yield the same parameter estimates. However, in practice we found improved results by fitting both functions simultaneously. The explanation for this is that the g function is especially sensitive at smaller scales r, but it approaches the asymptote $g = 1$ quickly at larger scales (compared with the way L approaches the asymptote 0). In turn, the accumulative L function is not very sensitive at small scales, but it is sensitive at larger scales. When optimizing both, the g and L functions produce, in general, more balanced fits than when using only the L function.

We first calculated the discrepancy between the model and the data separately for the g function (error g) and the L function (error L), and we minimized their geometric mean (error Lg):

$$\begin{aligned}
\text{error } L &= \frac{\sum_{r=r_0}^{r_{\max}} \left(\hat{L}(r)^c - L(r, \sigma, \rho)^c\right)^2}{\sum_{r=r_0}^{r_{\max}} \left(\hat{L}(r)^c\right)^2}, \\
\text{error } g &= \frac{\sum_{r=r_0}^{r_{\max}} \left(\hat{g}(r)^c - g(r, \sigma, \rho)^c\right)^2}{\sum_{r=r_0}^{r_{\max}} \left(\hat{g}(r)^c\right)^2}, \\
\text{error } Lg &= \sqrt{\text{error } g \times \text{error } L},
\end{aligned} \tag{A5}$$

with tuning constants r_0, $r_{\max}$, and c. The constant r_0 is the minimal scale of the fit, $r_{\max}$ is the maximal scale of the fit, and c is a power transformation. The error functions error g and error L give the fraction of the total sum of

squares of the transformed empirical g function and L function, respectively, which is not explained by the model. To fit the parameters, we minimize the average contrast error Lg of the g and L functions (eq. [A5]).

An immediate question is how to choose appropriate values for the tuning constants r_0, r_{max}, and c. A power transformation with $c > 1$ weights larger values of $L(r)$ or $g(r)$ more than one with $c = 1$, whereas a transformation with $c < 1$ weights larger differences less. We use in all analyses a power transformation with $c = 1$ for the L function and one with $c = 0.5$ for the g function to reduce the high sensitivity of the g function to smaller scales.

If we aim to fit the large-scale component of a double-cluster process (i.e., the parameters σ_1 and ρ_1 in eq. [A4]) using a Thomas process, comparison of the fitted Thomas process with the empirical pair-correlation function provides, in general, clear indications about the selection of r_0 if the critical scales of clustering are well separated (fig. A3*d*). The best approach, however, is to try several values for r_0 and visualize the g and L functions of the data and the fit. In our experience, it was not necessary to use minimal-contrast methods for determination of r_0.

A potential problem when using the L function for parameter estimation is that the accumulative L function has a memory (fig. A3*a*, A3*c*; Wiegand and Moloney 2004). The problem arises when fitting a Thomas process to a point pattern that shows an additional small-scale clustering. In this case, the observed values of the accumulative L function are influenced by this small-scale clustering, even for scales larger than the range of the small-scale clustering. This is illustrated in figure A3. The pair-correlation function, which is not affected by the memory, shows that the range of small-scale clustering is approximately 8 m (fig. A3*d*). This small-scale clustering makes the L function initially steeper than the L function of a Thomas process with only one critical scale of clustering (fig. A3*a*). As a consequence, the fit of a double-cluster L function with a Thomas process remains unsatisfactory, even when fitted only for scales larger than the range of small-scale clustering (i.e., $r = 8–50$ m; fig. A3*c*). Note that the fit with the pair-correlation function for scale of 8–50 m produces satisfactory results (fig. A3*d*). This is because the pair-correlation function is not accumulative. Thus, fitting the Thomas process with the L function to a pattern that shows two critical scales of clustering produces biased estimates of the parameters of the cluster process (Stoyan and Stoyan 1996) and leads to the observation that the parameter estimates depend, with sensitivity, on the upper limit r_{max} to which the K function is fitted (e.g., Batista and Maguire 1998; Plotkin et al. 2000).

To overcome this limitation, Wiegand et al. (2007*a*) developed a transformation of the K function that removes the memory. This transformation makes the value of the theoretical K function at r_0 equal to the observed value (i.e., it removes any memory; fig. A3*e*, *circle*). The transformed K function yields

$$K_t(r, r \geq r_0) = K_0 - K(r_0) + K(r), \tag{A6}$$

where K_0 is the observed value at scale r_0 (i.e., $\hat{K}(r_0) = K_0$) and $K(r_0)$ is the theoretical value of the common K function at scale r_0. We calculated the L function in the fitting procedure on the basis of the transformed K function instead of the common $K(r)$ function, which shows memory effects.

Separation of the scales of clustering (i.e., $\sigma_1^2 \gg \sigma_2^2$ in eq. [A4]) suggests a convenient approach to fitting the four parameters of the double-cluster process. In a first step, we fitted the parameters σ_{sum}^2 and ρ_1 of the overall larger-scale clustering using a Thomas process (eq. [A1]), but we fitted only for scales r that were larger than the range of the small-scale clustering (fig. A3*d*, A3*f*). We assessed the range of the small-scale clustering by comparing the plots of the estimated pair-correlation function and the fitted pair-correlation function (fig. A3*d*). In the second step, we used the estimates of σ_{sum}^2 and ρ_1 and fitted the two unknown parameters σ_2^2 and ρ_2 of the small-scale clustering using the full double-cluster model over the entire range of scales.

Decomposition of a Pattern into a Double-Cluster Component and a Random Component

The pair-correlation function of the double-cluster process (eq. [2]) and the double-cluster–random superposition process (eq. [4]) have the same functional form and therefore cannot be distinguished on the basis of the pair-correlation function alone. However, the distribution function of the nearest-neighbor distances reveals differences, because most points of a double-cluster pattern will have their nearest neighbor close by (i.e., within the same small-scale or large-scale cluster), whereas most points of the random-component pattern of a superposition pattern will be isolated, without their nearest neighbors being close by. The basic idea of the separation is therefore to determine isolated recruits that might belong to the random-component pattern.

To separate isolated points from clustered points, we first calculated the distance to the nearest neighbor for each recruit of a given recruitment generation (considering only recruits from the same census). Next we consulted the

distribution of nearest-neighbor distances $D(y)$ expected under a pure double-cluster process (i.e., the gray line and the simulation envelopes in fig. 2*A*) for an initial estimate of a suitable separation distance. All recruits without neighbors within the separation distance were assigned to the tentative random-component pattern. Note that this is not a perfect decomposition because some recruits of the random-component pattern may accidentally be located within a cluster and thus be unable to be detected. After determining for each census the two tentative component patterns, we joined the tentative component patterns of the different censuses in one tentative double-cluster pattern and one tentative random pattern. By analyzing the joined patterns, we therefore analyzed the spatial structure of all recruits within the 25 years covered by the censuses. However, when possible, we also analyzed the data sets of individual censuses to explore temporal effects. An interesting question that may shed light on the drivers of recruitment is whether subsequent recruitment generations are spatially independent or have a tendency to occur at the same places (see app. B).

Next we tested whether the tentative random-component pattern was, in good approximation, a random pattern, and whether the two tentative component patterns were, in good approximation, independent. If the initial separation distance was too small, some recruits that are actually members of the same cluster would be assigned to the random component. In this case, the tentative random pattern may show some clustering at smaller scales and the two component patterns will show attraction. On the other hand, if the separation distance was too large, the distribution function $D(y)$ of the nearest neighbor distances of the double-clustered component pattern would not fit well. We therefore tested several separation distances to find the best balance among these criteria.

When a reasonable separation distance was determined, we explored whether the double-cluster component can indeed be described with the double-cluster process, and we fitted equation (2) to the data. We then compared the parameter estimates of the double-cluster component pattern with those of the original noncomposed pattern: the estimates of σ should be the same, and the parameters ρ of the double-cluster component pattern should yield $\rho = \rho^* p_C^2$, where ρ^* is the corresponding fit for the original nondecomposed pattern and p_C is the proportion of recruits that belong to the clustered component pattern. Thus, our methodology provides five tests to assess whether the original pattern was a superposition of a random pattern and a pure double-cluster pattern: (1) the component pattern of isolated points should follow CSR, (2) the component of the clustered points should follow a double-cluster process, (3) the two component patterns should be independent, (4) the fitted values of the cluster sizes σ are the same, and (5) $\rho = \rho^* p_C^2$.

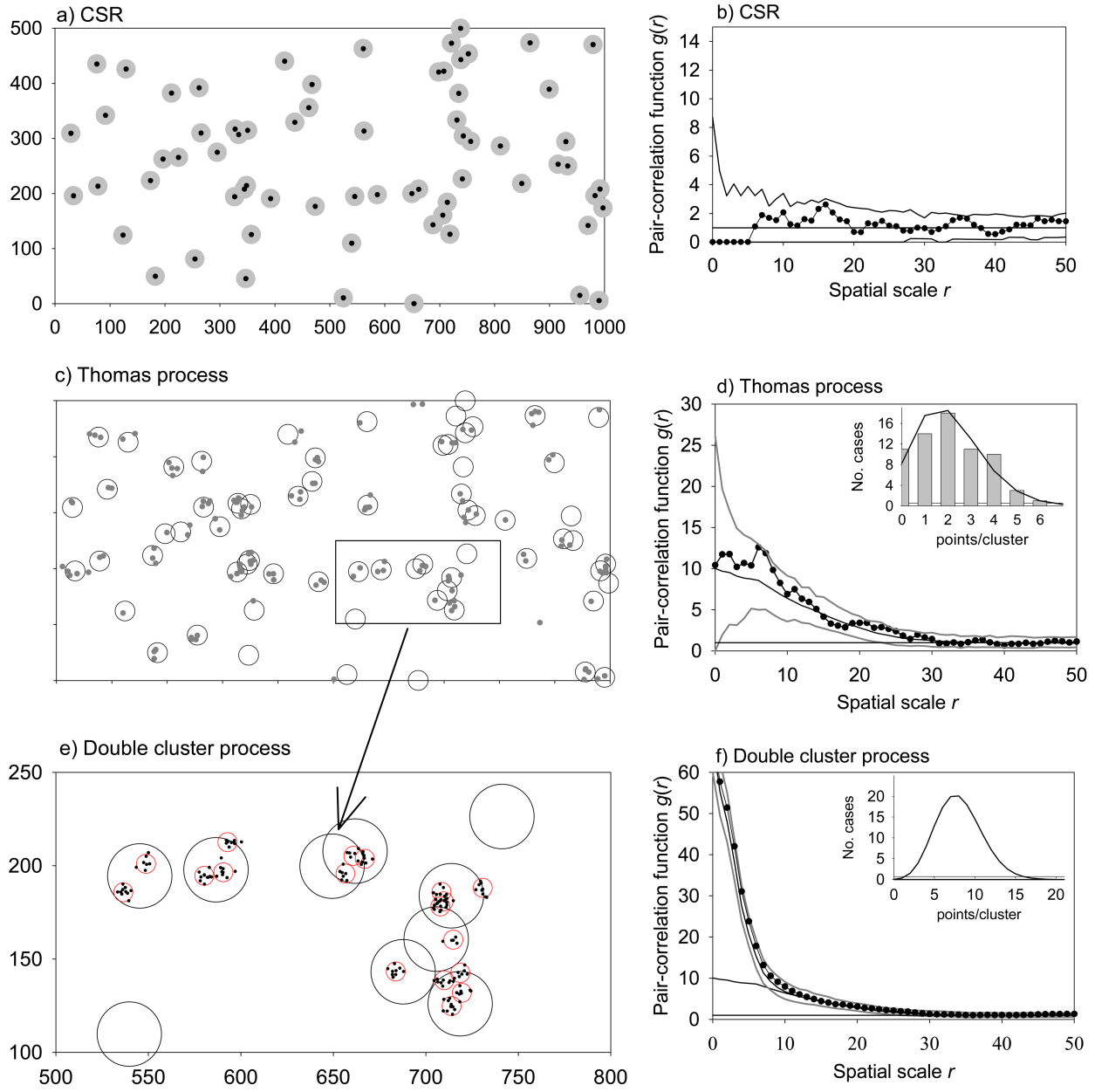

Figure A1: Example of the construction of cluster processes with one and two critical scales of clustering. *a*, Sixty-eight large clusters are randomly distributed over a 50-ha study area; the size of the gray disk corresponds to the approximate size of the clusters. *b*, Test with the pair-correlation function showing that the pattern of the cluster centers (*dots*) is indeed a random pattern. Shown here is the pair-correlation function of the pattern shown in *a* (*dots*), simulation envelopes (*black solid lines*) representing the fifth-lowest and -highest values of the pair-correlation function of 199 simulations of complete spatial randomness (CSR), and the expectation of the pair-correlation function (*solid horizontal line*). *c*, Point pattern generated with a Thomas process, where 144 points are randomly distributed over 68 clusters with parameter $\sigma = 6.5$ m. Note that some clusters are empty. *d*, Pair-correlation function (*dots*) of the point pattern shown in *c*, simulation envelopes (*black solid lines*) indicating the fifth-lowest and -highest values of the pair-correlation function of 199 simulations of the underlying Thomas process, and the expected pair-correlation function (*gray solid line*). The inset in *d* shows the distribution of the number of points per cluster (*bars* = data; *line* = expected). *e*, Part of a point pattern generated with a double-cluster process, where the points of the pattern shown in *c* become small clusters with parameter $\sigma = 2.7$ m and where 1,160 points are randomly distributed over 144 small clusters. *f*, Same as *d*, but for the pattern shown in *e*.

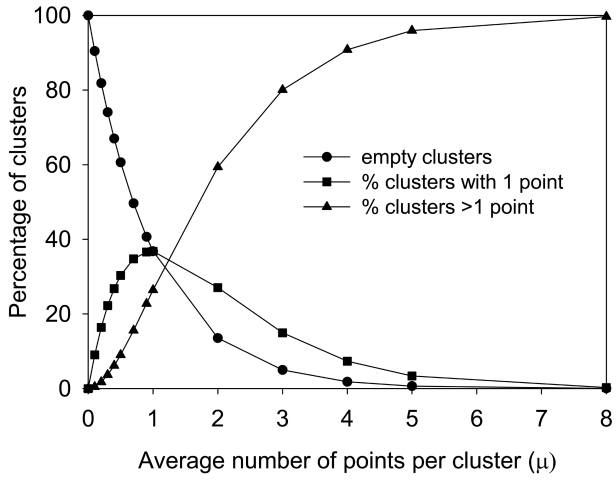

Figure A2: Dependence of the number of points per cluster on μ, the average number of points per cluster. Note that empty clusters may be frequent if $\mu < 2$.

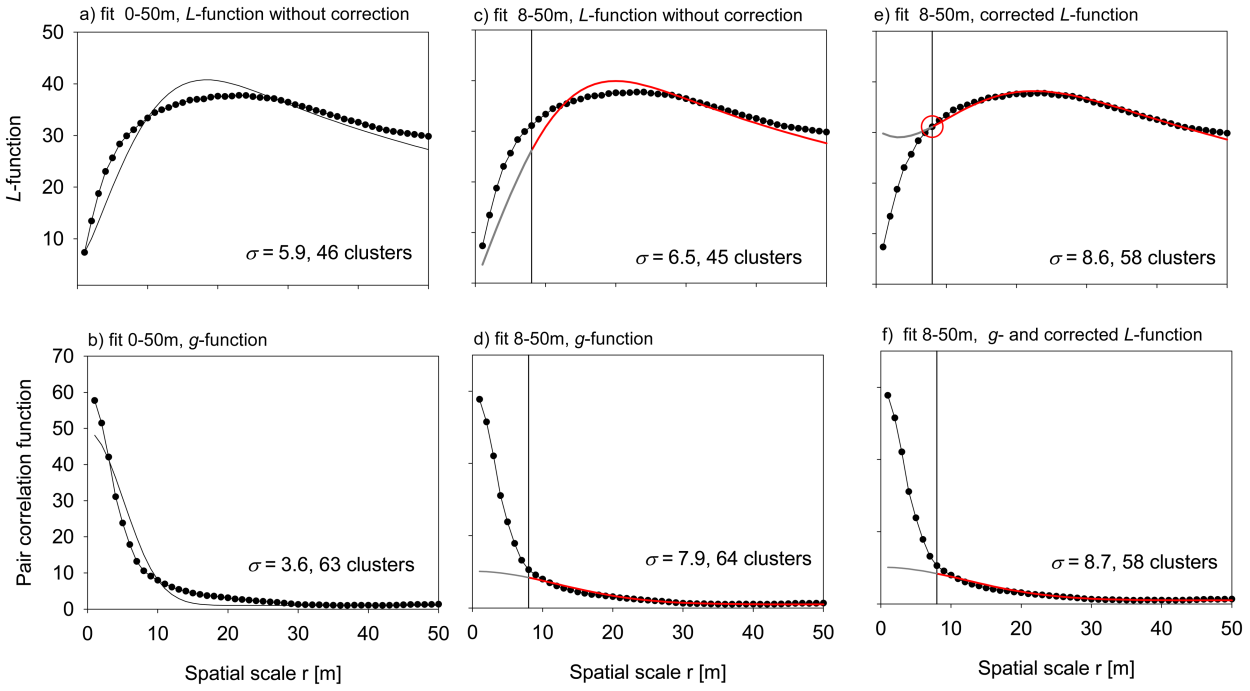

Figure A3: Memory of the accumulative L function may cause problems when fitting a Thomas process to point patterns with additional small-scale effects. *a*, Fit of a pattern generated by a double-cluster process with the Thomas process using the L function. The fit is not satisfactory. Dots indicate the observed L function; the line indicates the L function of the best fit with the Thomas process fitted for scale 0–50 m. *b*, Same as *a*, but using the pair-correlation function. *c*, Same as *a*, but fitted for scale 8–50 m. The fit is not satisfactory. *d*, Same as *c*, but with pair-correlation function. The fit is satisfactory. *e*, Fit for scales 8–50 m with transformed L function that removes the memory. The fit is satisfactory. *f*, Best fit minimizing the contrast for the L function and the g function simultaneously. The fit is satisfactory.

APPENDIX B

Detailed Description of the Analyses and Analysis of Recruitment Data from Different Censuses

Detailed Description of Analysis of Cecropia insignis

The pair-correlation function, which measures the neighborhood density of recruits relative to the density expected under a random pattern, reveals that the total *C. insignis* recruitment accumulated during the five census periods was highly aggregated (fig. 2). The density of recruits within 1 m of an average recruit was 50 times that expected by a random distribution (i.e., $g(r = 0) \approx 50$; fig. 2*A*), and neighborhood densities were elevated for distances of up to 40 m (i.e., $g(r) > 0$ for $r < 40$ m). The pair-correlation function can be fitted well with a double-cluster process: the observed pair-correlation function is within the simulation envelopes (fig. 2*A*), and the goodness-of-fit test for scales $r = 1–50$ m yielded a rank of 189 (table B1), indicating no significant departure between the fitted model and the data. The critical scale of large-scale clustering yields $r_{C1} = 17.2$ m, and that of small-scale clustering yields $r_{C2} = 5.3$ m. An average large cluster contained 2.2 small clusters (i.e., $\rho_2/\rho_1 = 2.2$), and an average small cluster contained 7 recruits (table 2).

The distribution function $D(y)$ of the distances y to the nearest neighbor, however, clearly showed that the pattern cannot be described by a pure double-cluster process (fig. 2*A*, *inset*), because in this case most recruits would have their nearest neighbor within the same small cluster (i.e., within distances $y < 5$ m). The observed $D(y)$ shows that a substantial proportion of recruits had their nearest neighbor at distances y that were much larger than expected under this null model (i.e., the observed $D(y)$ is substantially below the expected $D(y)$).

We therefore tested whether the pattern of recruits was a double-cluster–random superposition. To this end, we decomposed the original pattern of each recruitment generation of *C. insignis* into two components (see app. A): a "cluster component" pattern containing those recruits that had their nearest neighbor at distances smaller than a given separation distance (fig. 2*B*), and an "isolated component" pattern containing the rest, those recruits that had no nearest neighbor within the separation distance (fig. 2*E*). A distance of 8 m yielded the best separation. Eighty-six percent of the recruits (1,206 individuals) belonged to the cluster component pattern, and 14% (200 recruits) belonged to the isolated component pattern (table 2). Analysis of the cluster component pattern with the double-cluster process (eq. [2]) showed that the clustered recruit pattern can be fitted well with this process, except for some additional clustering at small scales $r < 2$ m (fig. 2*D*; table 2); the goodness-of-fit test for scales $r = 1–50$ m yielded a rank of 178. The best fit with the double-cluster process (eq. [2]) yielded critical scales of clustering of $r_{C1} = 16.6$ m and $r_{C2} = 5.3$ m, as well as 69 and 147 large and small clusters, respectively. Thus, an average large cluster of *C. insignis* contained 18 recruits that were distributed on average into two small clusters with approximately 8 recruits (table 2).

Comparing the estimates of the parameters ρ^* of the fit of the nondecomposed pattern with the parameters ρ of the cluster component showed that the process is likely to be a double-cluster–random superposition. We found that $(\rho_1/\rho_1^*)^{0.5} = (69/88)^{0.5} = 0.88$ and $(\rho_2/\rho_2^*)^{0.5} = (147/197)^{0.5} = 0.86$, which are in excellent agreement with the expectation of $p_C = 0.86$ (table 2). We also found that the empirical distribution function of distances to the nearest neighbor approximated the expectation under the null model reasonably well (see fig. 2*D*, *inset*; fig. 2*A*). The next step was to test whether the isolated component pattern could be approximated by a random pattern and whether it was independent from the clustered component pattern. Figure 2*F* shows that component pattern 2 was, in good approximation, a random pattern (rank, 192; 0–50 m), and the inset in figure 2*F* confirms that the two component patterns were independent (rank, 120; 0–50 m).

Separate analysis of the pooled 1985, 1990, and 1995 recruitment generations and the 2000 and the 2005 recruitment generations (fig. B1) provided additional interesting insight (the number of recruits during the first three censuses was too low to be analyzed separately). Recruitment during the 1985–1995 period was relatively low (some 100 recruits per census), but it increased strongly in 2000 and 2005 to 407 and 692 recruits per census, respectively. The proportion of isolated recruits was high during the 1985–1995 periods (31%), but it decreased to 6% and 12% for the 2000 and 2005 censuses, respectively (table 2). We found that the clustered component patterns followed double-cluster processes, with approximately two small clusters within one large cluster and critical scales of clustering that were practically identical for all recruitment generations (table 2). Interestingly, the clustered component patterns of different periods were independent (fig. B2), and the sum of the estimated numbers of large clusters (26, 14, and 34 for the first, second, and third period, respectively; table 2) approximates the number of clusters of the joined clustered component pattern well (69; table 2). Thus, the clusters of *C. insignis* were temporally and spatially independent.

Detailed Description of Analysis of Cordia bicolor

The pair-correlation function reveals that the >25 years of accumulated recruitment of *C. bicolor* was highly aggregated. The density of recruits within distances of <1 m was, at the western and eastern subplots, 15 and 40 times that expected by a random distribution (fig. 3*A*, 3*C*), respectively. The pair-correlation functions of the recruit patterns could be fitted well with a double-cluster process: the observed pair-correlation function is within the simulation envelopes (fig. 3*A*) and the goodness-of-fit test for scales $r = 1–50$ yielded for the western and eastern subplots ranks of 125 and 171 (table B1), respectively, indicating no significant departure between the fitted model and the data. The fitted parameters are shown in table 2: the critical scale of the large-scale clustering yields for the western and eastern subplots $r_{C1} = 20.0$ m and 21.5 m, respectively, and that of small-scale clustering $r_{C2} = 2.7$ m, and an average large cluster at the western and eastern subplots contained approximately 10 and three small clusters (i.e., ρ_2/ρ_1; table 2), respectively.

The distribution function $D(y)$ of the distances y to the nearest neighbor, however, clearly showed that the patterns cannot be described by a pure double-cluster process (fig. 3*A*, 3*C*, *inset*) because the observed $D(y)$ is below the expected $D(y)$. This suggests that the pattern of *C. bicolor* may be a superposition pattern. We therefore tested whether the pattern of recruits was a double-cluster–random superposition. A separation distance of 16 m yielded the best separation for both subplots.

Western subplot: At the western subplot there were 531 trees in the cluster-component pattern and 164 trees (24%) in the isolated-component pattern (table 2), yielding $p_C = 0.76$. Analysis of the cluster-component pattern with the double-cluster process (eq. [2]) showed that this pattern can be fitted well with this process (fig. 3*D*; table 2); the goodness-of-fit test for scales $r = 1–50$ yielded a rank of 71. The best fit with the double-cluster process (eq. [2]) yielded cluster sizes of $r_{C1} = 20.0$ m and $r_{C2} = 2.6$ m, and about 54 and 531 large and small clusters, respectively. Thus, an average large cluster of *Cecropia insignis* contained $\mu_1 = 9.8$ recruits that were distributed on average into $\rho_2/\rho_1 = 9.8$ small clusters containing on average one recruit (table 2). Comparing the estimates of parameters ρ with the number of clusters (where ρ^* indicates the estimates of the nonseparated pattern) allowed us to test whether the process is likely to be a double-cluster–random superposition. We found $(\rho_1/\rho_1^*)^{0.5} = (54/90)^{0.5} = 0.78$ and $(\rho_2/\rho_2^*)^{0.5} = (531/920)^{0.5} = 0.76$, which is in excellent agreement with the expectation $p_C = 0.76$. We also found that the empirical distribution function of distances to the nearest neighbor approximated the expectation under the null model reasonably well (see fig. 3*D*, *inset*; fig. 3*A*).

Eastern subplot: At the eastern subplot there were 113 trees in the cluster-component pattern and 96 trees (46%) in the isolated-component pattern (table 2), yielding $p_C = 0.54$. Analysis of the cluster-component pattern with the double-cluster process (eq. [2]) showed that this pattern can be fitted well with this process (fig. 3*F*; table 2); the goodness-of-fit test for scales $r = 1–50$ yielded a rank of 144. The best fit with the double-cluster process (eq. [2]) yielded cluster sizes of $r_{C1} = 20.0$ m and $r_{C2} = 2.8$ m and about 26 and 80 large and small clusters, respectively. Thus, an average large cluster of *C. insignis* contained $\mu_1 = 4.4$ recruits that were distributed on average into $\rho_2/\rho_1 = 3.1$ small clusters containing on average 1.4 recruits (table 2). We found $(\rho_1/\rho_1^*)^{0.5} = (26/69)^{0.5} = 0.61$ and $(\rho_2/\rho_2^*)^{0.5} = (80/283)^{0.5} = 0.53$, which is in excellent agreement with the expectation $p_C = 0.54$. We also found that the empirical distribution function of distances to the nearest neighbor approximated the expectation under the null model reasonably well (see fig. 3*F*, *inset*; fig. 3*C*).

The next step was to test whether the isolated recruit-component pattern could be approximated by a random pattern as assumed by the double-cluster–random superposition process and whether it was independent from the clustered-component pattern. Figure 3*G*, 3*I* shows that component patterns 2 were, in good approximation for both subplots, a random pattern, and that the insets in figure 3*G*, 3*I* show that the two component patterns were, in good approximation for both subplots, independent.

Interestingly, the random-component patterns from the two subplots formed one (homogeneous) random pattern (fig. 3*H*; the rank of the goodness-of-fit test for complete spatial randomness taken over scales $r = 0–50$ m yielded 175 for the g function and 150 for the D function). However, the average number of recruits per large cluster (μ_1) was twice as large at the western subplot than at the eastern subplot (table 2).

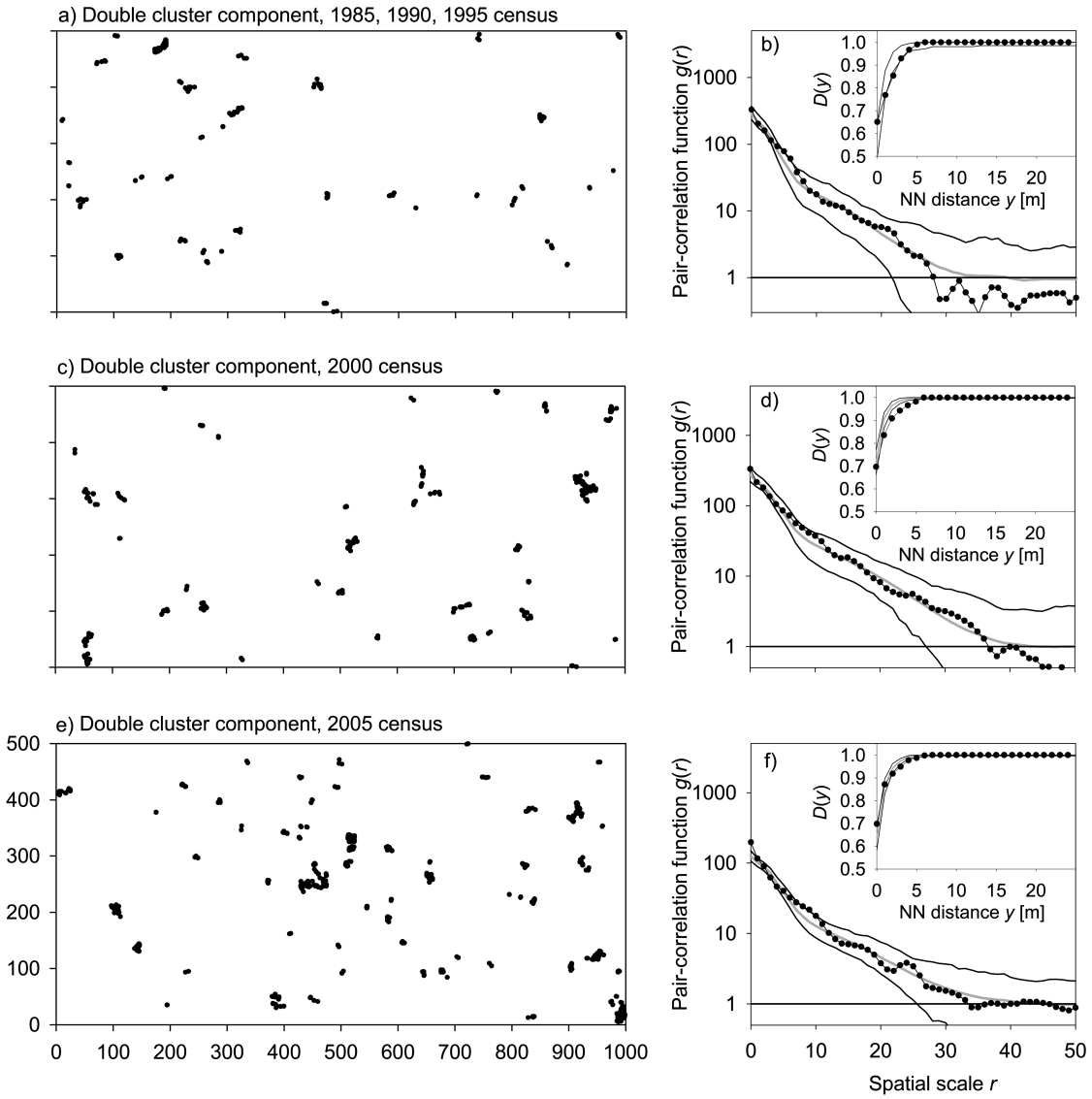

Figure B1: Detailed analysis of the data of *Cecropia insignis* recruitment from different censuses. We pooled the data from the 1985, 1990, and 1995 censuses because of the low numbers of recruits. *a*, *c*, and *e* show the double-clustered component pattern (all recruits that had their nearest same-generation neighbor within 8 m) for the 1985+1990+1995, 2000, and 2005 censuses, respectively. *b*, Pair-correlation function (*dots*), simulation envelopes (*black solid lines*) indicating the fifth-lowest and -highest values of the pair-correlation function of 199 simulations of the fitted double-cluster process (eq. [2]), and the fitted double-cluster pair-correlation function (*gray solid line*). The inset shows the empirical distribution $D(y)$ of the nearest-neighbor (NN) distances y (*dots*), the expected function of the null model (*gray solid line*), and the simulation envelopes (*black solid lines*). Note the logarithmic scale of the *Y*-axis. *d*, *f*, same as *b*, but for the 2000 and 2005 recruitment generations, respectively. $D(y)$ = cumulative distribution function of the distances y to the nearest neighbor.

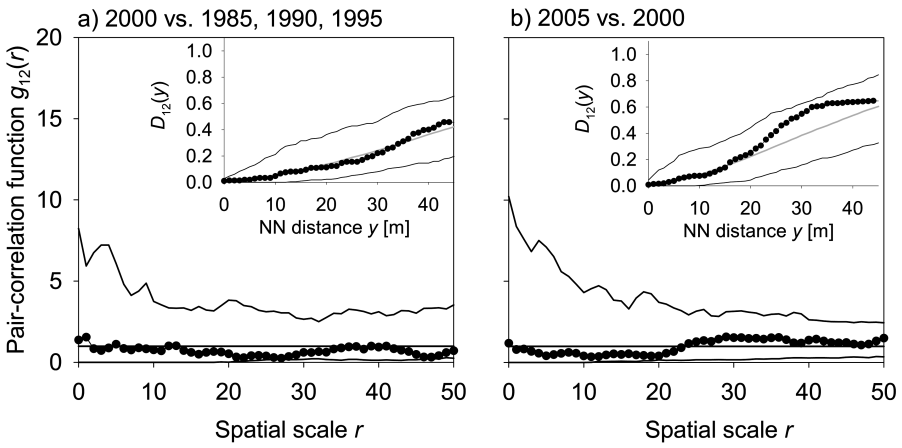

Figure B2: Test of independence of the double-cluster components of different *Cecropia insignis* recruitment generations (shown in fig. B1). *a*, Independence of the combined 1985+1990+1995 and the 2000 generations. *b*, Independence of the 2000 and 2005 generations. The pair-correlation function (*dots*) and simulation envelopes (*black solid lines*), which indicate the fifth-lowest and -highest values of the pair-correlation function of 199 simulations of the toroidal-shift null model testing for independence. The insets show the empirical distribution $D_{12}(y)$ of the nearest-neighbor (NN) distances y (*dots*), the expected function under the null model (*gray solid line*), and the simulation envelopes (*black solid lines*).

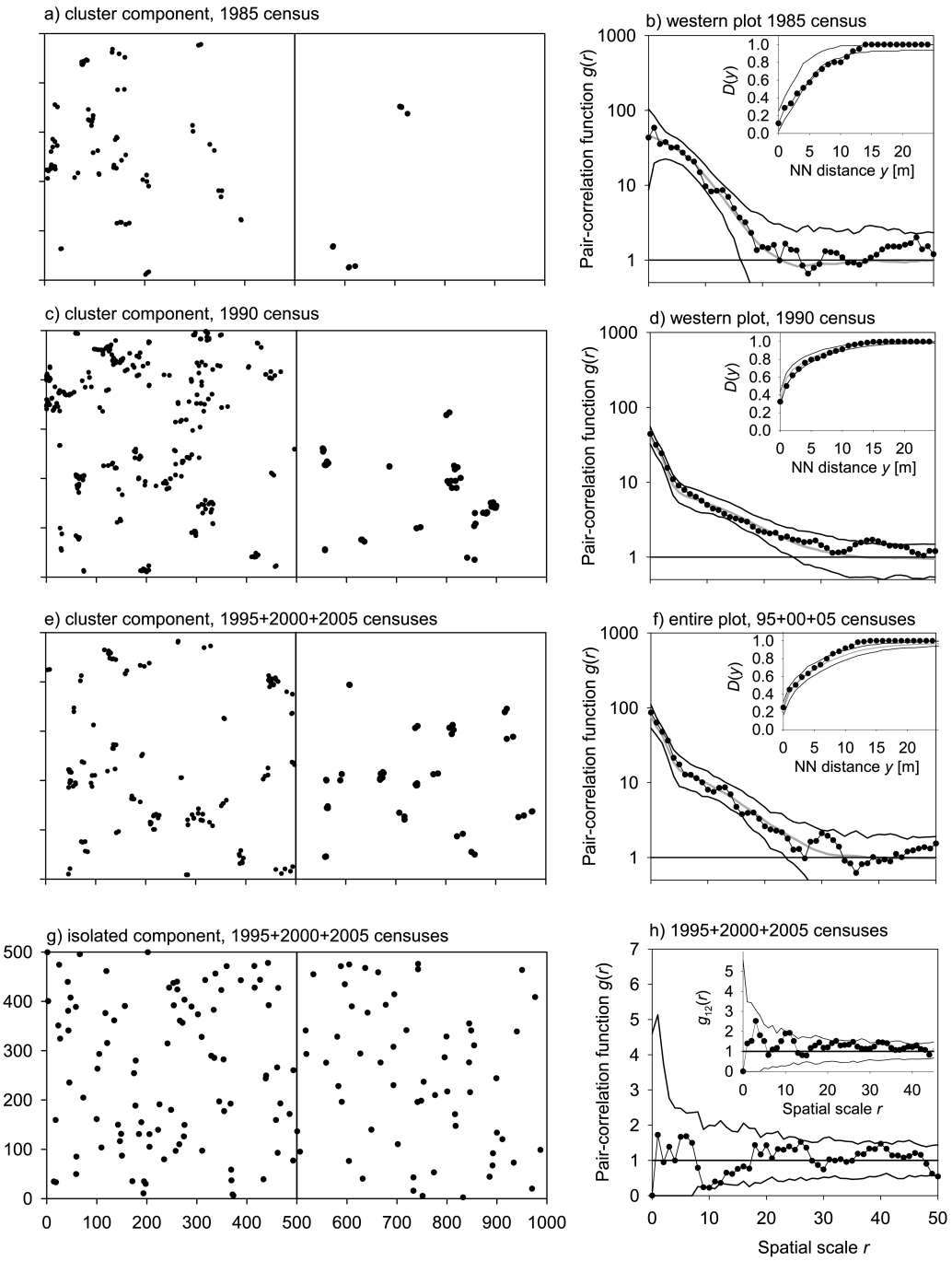

Figure B3: Detailed analysis of the cluster structure of different *Cordia bicolor* recruitment generations. We pooled the data from the 1995, 2000, and 2005 censuses because of the low numbers of recruits, and we performed the 1985 and 1990 census analyses separately for the western and eastern subplots. *a*, *c*, and *e* show the double-clustered component pattern (all recruits that had their same-generation nearest neighbor within 16 m) for the 1985, 1990, and combined 1995+2000+2005 censuses, respectively. *b*, Results for the western subplot of *a*. Note the logarithmic scale of the *Y*-axis. *d*, *f*, same as *b*, but for the 1990 and combined 1995+2000+2005 recruitment generations, respectively. *h*, Analysis of component pattern 2 with the complete spatial randomness null model. The inset shows the test of independence between the two component patterns. Other conventions are as they are in figure B1.

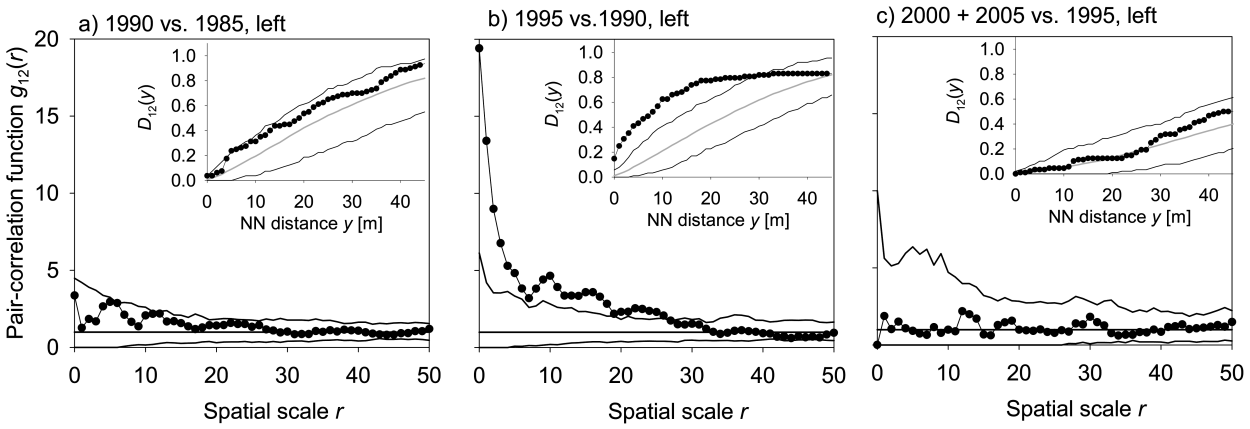

Figure B4: Test of independence of the double-cluster components of subsequent *Cordia bicolor* recruitment generations (shown in fig. B3). *a*, Independence of the 1985 and 1990 generations; *b*, independence of the 1990 and 1995 generations; and *c*, independence of the 1995 and combined 2000+2005 generations. Other conventions are as they are in figure B2.

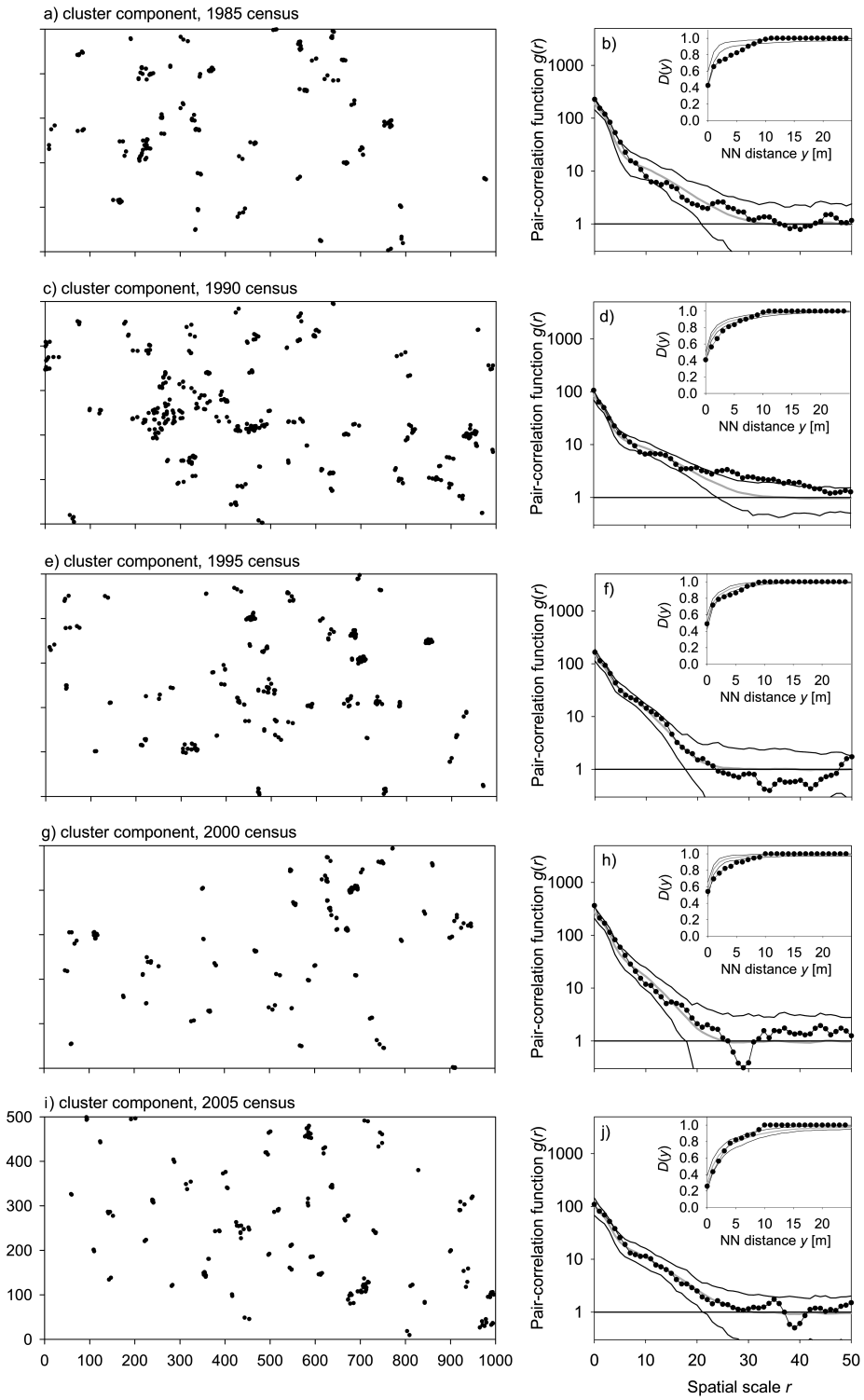

Figure B5: Detailed analysis of the cluster structure of different *Miconia argentea* recruitment generations. *a*, *c*, *e*, *g*, and *i* show the double-clustered component pattern (all recruits that had their same-generation nearest neighbor within 12 m) for the 1985, 1990, 1995, 2000, and 2005 censuses,

respectively. *b*, *d*, *f*, *h*, and *j* show the results for the patterns shown in panels *a*, *c*, *e*, *g*, and *i*, respectively. Note the logarithmic scale of the *Y*-axes. Other conventions are as they are in figure B1.

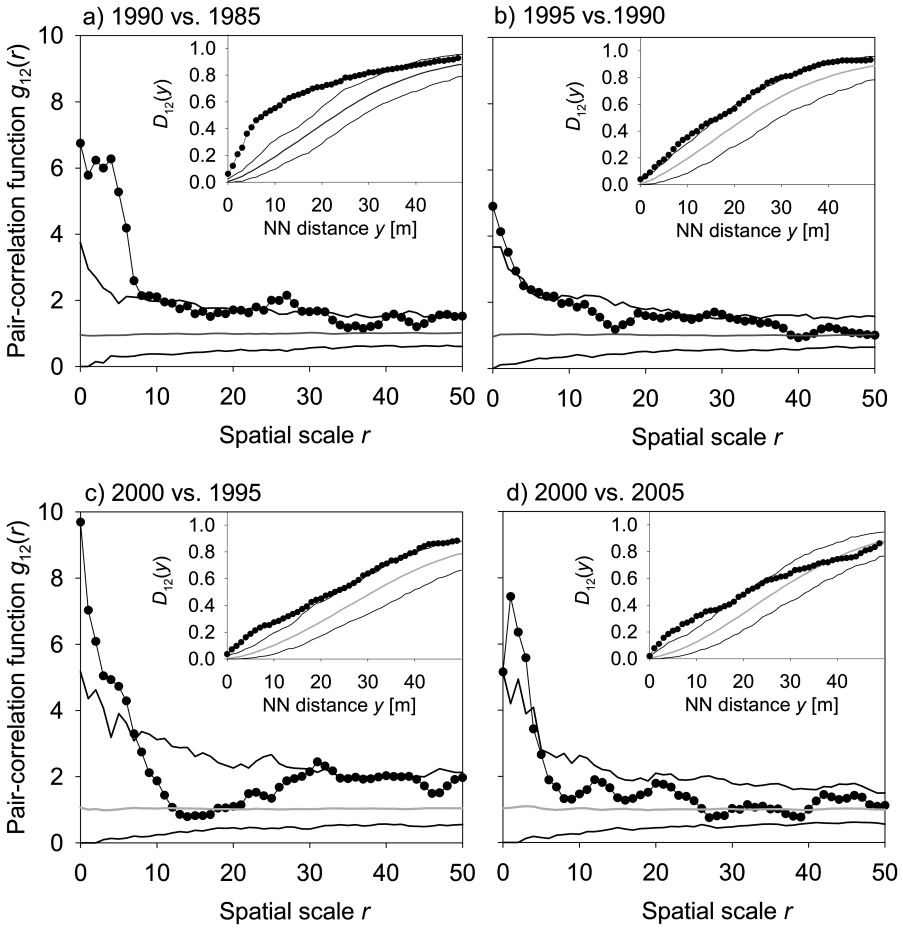

Figure B6: Test of independence of the pattern of subsequent *Miconia argentea* recruitment generations (as shown in fig. B5). Other conventions are as they are in figure B2.

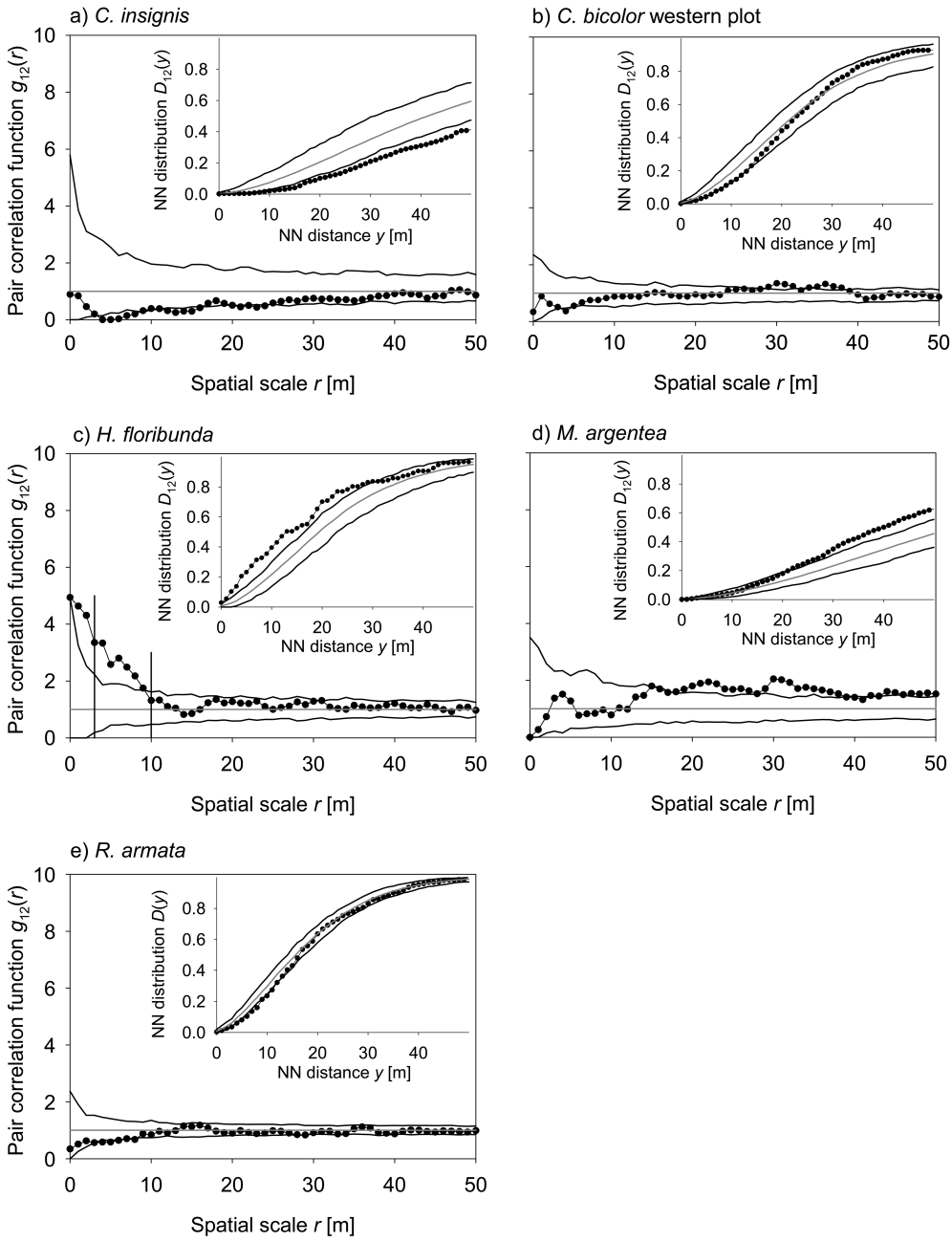

Figure B7: Relationship between the clustered-component patterns of recruits and the corresponding pattern of reproductive trees. We contrasted the observed functions $g_{12}(r)$ and $D_{12}(y)$ to approximate 95% simulation envelopes constructed from 199 simulations of the toroidal shift null model, where the adults were moved relative to the recruits pattern. The main figures show the results of the analysis with the pair-correlation function $g_{12}(r)$, and the insets show the cumulative distribution function $D_{12}(y)$ of the distances y of the recruits to the nearest adult. The dots show the observed functions, the solid gray line shows the expectation under the null model, and the solid black lines show the simulation envelopes. The vertical lines in *c* show the critical scales of clustering (table 2).

Table B1: Rank and range of scales used for the goodness-of-fit test for the different analyses

Species, component	Scale (m)	Rank $g(r)$	Scale s (m)	Rank $D(r)$	Figure
Cecropia insignis, all censuses:					
All recruits	1–50	189	1–50	200	2*A*
Cluster	1–50	178	1–50	200	2*D*
Isolated CSR	0–50	192	0–50	200	2*F*
Independence	0–50	120	0–50	200	2*F*, *inset*
C. insignis, single census:					
1985+1990+1995 cluster	0–50	150	0–50	197	B1*b*
2000 cluster	0–50	168	0–50	200	B1*d*
2005 cluster	1–50	182	1–50	192	B1*f*
Cordia bicolor western, all censuses:					
All recruits	0–50	95	0–50	200	3*A*
Cluster component	0–50	35	0–50	200	3*D*
Isolated CSR	0–50	187	0–50	187	3*G*
Independence	0–50	100	0–50	194	3*G*, *inset*
C. bicolor eastern, all censuses:					
All recruits	0–50	136	0–50	200	3*C*
Cluster	0–50	107	0–50	199	3*F*
Isolated CSR	0–50	10	0–50	192	3*I*
Independence	0–50	161	0–50	96	3*I*, *inset*
C. bicolor all, all censuses:					
Isolated CSR	0–50	175	0–50	150	3*H*
C. bicolor western, single census					
1985 cluster	0–50	32	0–50	195	B3*b*
1990 cluster	0–50	51	0–50	191	B3*d*
1995+2000+2005 cluster	0–50	6	…	124	…
C. bicolor entire plot 1995+2000+2005:					
Cluster	…	70	…	199	B3*f*
Isolated CSR	0–50	59	0–50	66	B3*h*, *inset*
Independence	0–50	143	0–50	97	B3*h*
Miconia argentea, all censuses:					
All recruits	1–20	144	0–50	200	4*A*
Cluster	1–20	192	0–50	200	4*D*
Isolated CSR	0–50	178	0–50	110	4*F*
Independence	0–50	200	0–50	196	4*F*, *inset*
M. argentea, single census:					
1985 cluster	0–50	182	0–50	200	B5*b*
1990 cluster	1–50	141	0–50	200	B5*d*
1995 cluster	0–50	135	0–50	199	B5*f*
2000 cluster	1–50	118	0–50	200	B5*h*
2005 cluster	0–50	71	0–50	199	B5*j*
Hasseltia floribunda, all censuses	1–50	2	0–50	198	5*A*
Randia armata, all censuses	0–50	9	0–50	18	5*C*

Note: CSR = complete spatial randomness.

Table B2: Rank of goodness-of-fit test for the different analyses regarding independence of the recruit pattern of subsequent censuses

Species, census pattern 1	Census pattern 2	Rank $g_{12}(r)$	Rank $D_{12}(r)$	Figure
Cecropia insignis:				
1985–1995	2000	5	7	B2*a*
2000	2005	44	74	B2*b*
Cordia bicolor western:				
1985	1990	183	152	B4*a*

Table B2 (*Continued*)

Species, census pattern 1	Census pattern 2	Rank $g_{12}(r)$	Rank $D_{12}(r)$	Figure
1990	1995	200	200	B4*b*
1995	2000 + 2005	0	74	B4*b*
Miconia argentea:				
1985	1990	200	200	B6*a*
1990	1995	197	194	B6*b*
1995	2000	199	199	B6*c*
2000	2005	196	195	B6*d*

Note: The test interval of the goodness-of-fit test was 0–50 m in all cases.

Table B3: Rank and range of the goodness-of-fit test for the different analyses regarding independence of the recruit pattern and the pattern of reproductive trees

Species	Rank $g_{12}(r)$	Rank $D_{12}(r)$	Figure
Cecropia insignis	173	200	B7*a*
Cordia bicolor western	162	124	B7*b*
Hasseltia floribunda	200	200	B7*c*
Miconia argentea	195	200	B7*d*
Randia armata	179	176	B7*e*

APPENDIX C

Combining the Data from Individual Mapped Replicate Plots into Mean Weighted Test Statistics

The data on the bivariate adult-recruit patterns from different censuses are statistics replicates that are created by the same underlying process. To summarize the data in an effective way, we can combine the test statistics of individual censuses into average second-order statistics (Diggle 2003; Illian et al. 2008). Because the pair-correlation function (as well as the K function) is itself defined as a ratio, $g(r) = O(r)/\lambda$, a good strategy is to separately pool estimates of λ and $O(r) = \lambda g(r)$ (Diggle 2003, p. 123).

As such, we first developed the weighted estimators of the O-ring statistic $O_{12}(r)$ and the intensity λ_2 of pattern 2, and then we used the relation $O_{12}(r) = \lambda_2 g_{12}(r)$ to estimate the pair-correlation function $g_{12}(r)$. Using the grid-based estimators of Programita and following the notation in Wiegand and Moloney (2004; their eq. [11]), the numerical estimator of the bivariate O-ring statistic $O_{12}(r)$ is calculated as

$$\hat{O}^{\mathrm{w}}_{12}(r) = \frac{(1/n_1)\sum_{i=1}^{n_1} \mathbf{Points_2}(R^{\mathrm{w}}_{1,i}(r))}{(1/n_1)\sum_{i=1}^{n_1} \mathbf{Area}(R^{\mathrm{w}}_{1,i}(r))}, \tag{C1}$$

where n_1 is the number of points of pattern 1, $R^{w}_{1,i}(r)$ is the ring with radius r and width w centered in the ith point of pattern 1, $\mathbf{Points_2}(x)$ counts the points of pattern 2 in a region x, and the operator $\mathbf{Area}(x)$ determines the area of the region x.

To integrate the data of M different replicates into a single weighted O-ring statistic, the formula for one replicate (eq. [C1]) is extended by calculating, for each spatial scale r, the average weighted number of points of pattern 2 taken over all M replicates and the average weighted area taken over all M replicates:

$$\hat{O}^{\mathrm{w}}_{12}(r) = \frac{\left\{\left(n^1_1/N\right)\left[\left(1/n^1_1\right)\sum_{i^1=1}^{n^1_1} \mathbf{Points_2}\left(R^{\mathrm{w}}_{1,i^1}(r)\right)\right] + \cdots + \left(n^M_1/N\right)\left[\left(1/n^M_1\right)\sum_{i^M=1}^{n^M_1} \mathbf{Points_2}\left(R^{\mathrm{w}}_{1,i^M}(r)\right)\right]\right\}}{\left\{\left(n^1_1/N\right)\left[\left(1/n^1_1\right)\sum_{i^1=1}^{n^1_1} \mathbf{Area}\left(R^{\mathrm{w}}_{1,i^1}(r)\right)\right] + \cdots + \left(n^M_1/N\right)\left[\left(1/n^M_1\right)\sum_{i^M=1}^{n^M_1} \mathbf{Area}\left(R^{\mathrm{w}}_{1,i^M}(r)\right)\right]\right\}}, \tag{C2}$$

where i^j is the ith point of pattern 1 and replicate j, n_1^j is the number of points of pattern 1 and replicate j, and $N = \sum_j n_1^j$ is the total number of points of pattern 1 in all replicates. Equation (C2) simplifies to

$$\hat{O}_{12}^{w}(r) = \frac{\sum_{i^1=1}^{n_1^1} \mathbf{Points}_2\left(R_{1,i^1}^{w}(r)\right) + \cdots + \sum_{i^M=1}^{n_1^M} \mathbf{Points}_2(R_{1,i^M}^{w}(r))}{\sum_{i^1=1}^{n_1^1} \mathbf{Area}\left(R_{1,i^1}^{w}(r)\right) + \cdots + \sum_{i_1^M=1}^{n_1^M} \mathbf{Area}(R_{1,i^M}^{w}(r))}. \tag{C3}$$

We estimate the overall intensity λ_2 as

$$\lambda_2 = \frac{\sum_{j=1}^{M} n_2^j}{\sum_{j=1}^{M} A^j}, \tag{C4}$$

where A^j is the area of replicate j. The estimator of the single weighted pair-correlation function is then given as

$$\hat{g}_{12}^{w}(r) = \frac{1}{\lambda_2} \hat{O}_{12}^{w}(r). \tag{C5}$$

APPENDIX D

Species Properties versus Cluster Characteristics

Table D1: Rank correlations between species properties and model parameters for fits of data of individual census periods (table 2)

Species property	Growth	Light	Dispersal	Weight	p_C	μ_1	μ_2	σ_1	σ_2	ρ_2/ρ_1	σ_1/σ_2
eff[a]	.90*	1.00**	−.10	−.70	−.56	.90*	1.00**	−.70	.10	−.70	−1.00**
Maximum sapling growth[b]	…	.90*	−.20	−.40	−.35	.63*	.64*	−.03	.25	−.37	−.60*
Light sensitivity[b]	…	…	−.10	−.70	−.12	.88**	.94**	−.40	.41	−.78**	−.93**
Mean dispersal distance[b]	…	…	…	.40	−.28	−.18	−.18	−.61*	−.70**	.23	.20
Seed weight[b]	…	…	…	…	−.21	−.73**	−.84**	.19	−.62*	.83**	.86**
p_C[c]	…	…	…	…	…	.07	−.04	.58*	.32	.1	.24
μ_1[c]	…	…	…	…	…	…	.90**	−.21	.2	−.48	−.75**
μ_2[c]	…	…	…	…	…	…	…	−.36	.37	−.75**	−.85**
σ_1[c]	…	…	…	…	…	…	…	…	.32	.36	.54
σ_2[c]	…	…	…	…	…	…	…	…	…	−.58*	−.45
ρ_2/ρ_1[c]	…	…	…	…	…	…	…	…	…	…	.80**

Note: p_C = proportion of recruits in the cluster-component pattern. μ_1 and μ_2 are the average numbers of trees in one large-scale and one small-scale cluster, respectively; $2\sigma_1$ and $2\sigma_2$ are the cluster sizes of the large and small clusters, respectively; and ρ_2/ρ_1 is the average number of small clusters in one large cluster.

[a] Index *eff* is a crude measure of dispersal quantity calculated as the number of defecations containing at least one seed of a particular tree species divided by the number of adults of that tree species in the Barro Colorado Island plot, based on data published in table 1 in Wehncke et al. (2003). Because the data on defecations were collected in 1999, we related *eff*-only cluster characteristics of the 2005 census.

[b] See table 1.

[c] See table 2.

* $P < .05$.

** $P < .01$.

Literature Cited

Amarasekare, P. 2003. Competitive coexistence in spatially structured environments: a synthesis. Ecology Letters 6:1109–1122.

Baddeley, A., J. Møller, and R. Waagepetersen. 2000. Non- and semi-parametric estimation of interaction in inhomogeneous point patterns. Statistica Neerlandica 54:329–350.

Barot, S., J. Gignoux, and J. C. Menaut. 1999. Demography of a savanna palm tree: predictions from comprehensive spatial pattern analyses. Ecology 80:1987–2005.

Batista, J. L. F., and D. A. Maguire. 1998. Modeling the spatial structure of tropical forests. Forest Ecology and Management 110:293–314.

Bolker, B. M., and S. W. Pacala. 1999. Spatial moment equations for plant competition: understanding spatial strategies and the advantages of short dispersal. American Naturalist 153:575–602.

Carlo, T. A., and J. M. Morales. 2008. Inequalities in fruit-removal and seed dispersal: consequences of bird behavior, neighbourhood density and landscape aggregation. Journal of Ecology 96:609–618.

Chesson, P. 2000. Mechanisms of maintenance of species diversity. Annual Review of Ecology, Evolution, and Systematics 31:343–366.

Chesson, P., M. J. Donahue, B. A. Melbourne, and A. L. W. Sears. 2005. Scale transition theory for understanding mechanisms in metacommunities. Pages 279–306 *in* M. Holyoak, M. A. Leibold, and R. D. Holt, eds. Metacommunities: spatial dynamics and ecological communities. University of Chicago Press, Chicago.

Clark, J. S., B. Beckage, P. Camill, B. Cleveland, J. HilleRisLambers, J. Lichter, J. McLachlan, J. Mohan, and P. Wyckoff. 1999*a*. Interpreting recruitment limitation in forests. American Journal of Botany 86:1–16.

Clark, J. S., M. Silman, R. Kern, E. Macklin, and J. HilleRisLambers. 1999*b*. Seed dispersal near and far: patterns across temperate and tropical forests. Ecology 80:1475–1494.

Comita, L. S., R. Condit, and S. P. Hubbell. 2007*a*. Developmental changes in habitat associations of tropical trees. Journal of Ecology 95:482–492.

Comita, L. S., S. Aguiar, R. Pérez, S. Lao, and S. P. Hubbell. 2007*b*. Patterns of woody plant species abundance and diversity in the seeding layer of a tropical forest. Journal of Vegetation Science 18: 163–174.

Condit, R. 1998. Tropical forest census plots. Springer, Berlin, and Landes, Georgetown.

Condit, R., P. S. Ashton, P. Baker, S. Bunyavejchewin, S. Gunatilleke, N. Gunatilleke, S. P. Hubbell, et al. 2000. Spatial patterns in the distribution of tropical tree species. Science 288:1414–1418.

Connell, J. H. 1971. On the role of natural enemies in preventing competitive exclusion in some marine animals and in rain forest trees. Pages 298–312 *in* P. J. Den Boer and G. Gradwell, eds. Dynamics of populations. PUDOC, Wageningen.

Croat, T. B. 1978. Flora of Barro Colorado Island. Stanford University Press, Stanford, CA.

Dalling, J. W., M. D. Swaine, and N. C. Garwood. 1998. Dispersal patterns and seed bank dynamics of pioneer trees in moist tropical forest. Ecology 79:564–578.

Dalling, J. W., H. C. Muller-Landau, S. J. Wright, and S. P. Hubbell. 2002. Role of dispersal in the recruitment limitation of Neotropical pioneer species. Journal of Ecology 90:714–727.

Dennis, A. J., and D. A. Westcott. 2007. Estimating dispersal kernels produced by a diverse community of vertebrates. Pages 201–228 *in* A. J. Dennis, R. J. Green, E. W. Schupp, and D. A. Westcott, eds. Seed dispersal: theory and its application in a changing world. CAB International, Wallingford.

Diggle, P. J. 2003. Statistical analysis of point patterns. 2nd ed. Arnold, London.

Fragoso, J. M. V. 1997. Tapir-generated seed shadows: scale dependent patchiness in the Amazon rain forest. Journal of Ecology 85:519–529.

———. 2005. The role of trophic interactions in community initiation, maintenance and degradation. Pages 310–327 *in* D. F. R. P. Burslem, M. A. Pinard, and S. Hartley, eds. Biotic interactions in the tropics. Cambridge University Press, Cambridge.

Fragoso, J. M. V., K. M. Silvius, and J. A. Correa. 2003. Long-distance seed dispersal by tapirs increases seed survival and aggregates tropical trees. Ecology 84:1998–2006.

Gallery, R. E., J. W. Dalling, B.T. Wolfe, and A. E. Arnold. 2007. The influence of seed source, habitat, and fungi on *Cecropia* seed survival in two Neotropical forests. Pages 479–498 *in* A. J. Dennis, R. Green, E. W. Schupp, and D. A. Westcott, eds. Seed dispersal: theory and its application in a changing world. CAB International, Wallingford.

Getzin, S., T. Wiegand, K. Wiegand, and F. He. 2008. Heterogeneity influences spatial patterns and demographics in forest stands. Journal of Ecology 96:807–820.

Goreaud, F., and R. Pélissier. 2003. Avoiding misinterpretation of biotic interactions with the intertype K-12-function: population independence vs. random labelling hypotheses. Journal of Vegetation Science 14:681–692.

Grimm, V., E. Revilla, U. Berger, F. Jeltsch, W. Mooij, S. F. Railsback, H. Thulke, J. Weiner, T. Wiegand, and D. L. DeAngelis. 2005. Pattern-oriented modeling of agent-based complex systems: lessons from ecology. Science 310:987–991.

Hampe, A., J. L. García-Castaño, E. W. Schupp, and P. Jordano. 2008. Spatio-temporal dynamics and local hotspots of initial recruitment in vertebrate-dispersed trees. Journal of Ecology 96:668–678.

Harms, K. E., R. Condit, S. P. Hubbell, and R. B. Foster. 2001. Habitat associations of trees and shrubs in a 50-ha Neotropical forest plot. Journal of Ecology 89:974–959.

He, F., P. Legendre, and J. V. LaFrankie. 1997. Distribution patterns of tree species in a Malaysian tropical rain forest. Journal of Vegetation Science 8:105–114.

Howe, H. F. 1989. Scatter- and clump-dispersal and seedling demography: hypothesis and implications. Oecologia (Berlin) 79: 417–426.

Howe, H. F., and J. Smallwood. 1982. Ecology of seed dispersal. Annual Review of Ecology, Evolution, and Systematics 13:201–228.

Hubbell, S. P. 2001. The unified neutral theory of biodiversity and biogeography. Princeton University Press, Princeton, NJ.

Hubbell, S. P., and R. B. Foster. 1983. Diversity of canopy trees in Neotropical forest and implications for conservation. Pages 25–41 *in* S. Sutton, T. Whitmore, and A. Chadwick, eds. Tropical rain forest: ecology and management. Blackwell Scientific, London.

Hubbell, S. P., R. B. Foster, S. T. O'Brien, K. E. Harms, R. Condit, B. Wechsler, S. J. Wright, and S. Loo de Lao. 1999. Light gap disturbances, recruitment limitation, and tree diversity in a Neotropical forest. Science 283:554–557.

Hubbell, S. P., R. Condit, and R. B. Foster. 2005. Barro Colorado Forest census plot data. http://ctfs.si.edu/datasets/bci.

Hurtt, G. C., and S. W. Pacala. 1995. The consequences of recruitment limitation: reconciling chance, history and competitive differences between plants. Journal of Theoretical Biology 176:1–12.

Illian, J., A. Penttinen, H. Stoyan, and D. Stoyan. 2008. Statistical analysis and modelling of spatial point patterns. Wiley, Chichester.

Janzen, D. H. 1970. Herbivores and the number of tree species in tropical forests. American Naturalist 104:501–528.

Kwit, C., D. J. Levey, S. A. Turner, C. J. Clark, and J. R. Poulsen. 2007. Out of one shadow and into another: causes and consequences of spatially contagious seed dispersal by frugivores. Pages 427–444 *in* A. J. Dennis, E. W. Schupp, R. J. Green, and D. A.

Westcott, eds. Seed dispersal: theory and its application in a changing world. CAB International, Wallingford.

Leigh, E. G. 1999. Tropical forest ecology: a view from Barro Colorado Island. Oxford University Press, New York.

Levey, D. J., J. J. Tewksbury, and B. M. Bolker. 2008. Modeling and measuring long-distance dispersal in a landscape context. Journal of Ecology 96:599–608.

Levin, S. A. 1992. The problem of pattern and scale in ecology. Ecology 73:1943–1967.

Loosmore, N. B., and E. D. Ford. 2006. Statistical inference using the G or K point pattern spatial statistics. Ecology 87:1925–1931.

McIntire, E. J. B., and A. Fajardo. 2009. Beyond description: the active and effective way to infer processes from spatial patterns. Ecology 90:46–56.

Muller-Landau, H. C., and B. D. Hardesty. 2005. Seed dispersal of woody plants in tropical forests: concepts, examples, and future directions. Pages 268–309 *in* D. F. R. P. Burslem, M. A. Pinard, and S. Hartley, eds. Biotic interactions in the tropics. Cambridge University Press, Cambridge.

Muller-Landau, H. C., S. J. Wright, O. Calderón, R. Condit, and S. P. Hubbell. 2008. Interspecific variation in primary seed dispersal in a tropical forest. Journal of Ecology 96:653–667.

Murrell, D. J., D. W. Purves, and R. Law. 2001. Uniting pattern and process in plant ecology. Trends in Ecology & Evolution 16:529–530.

Nathan, R., and H. C. Muller-Landau. 2000. Spatial patterns of seed dispersal, their determinants and consequences for recruitment. Trends in Ecology & Evolution 15:278–285.

Pacala, S. W. 1997. Dynamics of plant communities. Pages 532–555 *in* M. J. Crawley, ed. Plant ecology. 2nd ed. Blackwell Scientific, Oxford.

Passos, L. and P. S. Oliveira. 2002. Ants affect the distribution and performance of seedlings of *Clusia criuva*, a primarily bird-dispersed rain forest tree. Journal of Ecology 90:517–528.

Plotkin, J. B., M. D. Potts, N. Leslie, N. Manokaran, J. V. LaFrankie, and P. S. Ashton. 2000. Species-area curves, spatial aggregation, and habitat specialization in tropical forests. Journal of Theoretical Biology 207:81–99.

Plotkin, J. B., J. Chave, and P. S. Ashton. 2002. Cluster analysis of spatial patterns in Malaysian tree species. American Naturalist 160: 629–644.

Purves, D. W., and R. Law. 2002. Fine-scale spatial structure in a grassland community: quantifying the plant's-eye view. Journal of Ecology 90:121–129.

Ribbens, E., J. A. Silander, and S. W. Pacala. 1994. Seedling recruitment in forests: calibrating models to predict patterns of tree seedling dispersion. Ecology 75:1794–1806.

Rüger, N., A. Huth, S. P. Hubbell, and R. Condit. 2009. Response of recruitment to light availability across a tropical lowland rainforest community. Journal of Ecology (forthcoming). DOI: 10.1111/j.1365-2745.2009.01552.x.

Russo, S. E., and C. K. Augspurger. 2004. Aggregated seed dispersal by spider monkeys limits recruitment to clumped patterns in *Virola calophylla*. Ecology Letters 7:1058–1067.

Russo, S. E., S. Portnoy, and C. K. Augspurger. 2006. Incorporating animal behavior into seed dispersal models: implications for seed shadows. Ecology 87:3160–3174.

Schupp, E. W., T. Milleron, and S. E. Russo. 2002. Dissemination limitation and the origin and maintenance of species-rich tropical forests. Pages 19–33 *in* D. J. Levey, W. R. Silva, and M. Galetti, eds. Seed dispersal and frugivory: ecology, evolution and conservation. CAB International, Wallingford.

Seidler, T. G., and J. B. Plotkin. 2006. Seed dispersal and spatial pattern in tropical trees. PLoS Biology 4:2132–2137.

Stoyan, D., and H. Stoyan. 1994. Fractals, random shapes and point fields: methods of geometrical statistics. Wiley, Chichester.

———. 1996. Estimating pair correlation functions of planar cluster processes. Biometrical Journal 38:259–271.

Svenning, J. C., B. M. J. Engelbrecht, D. A. Kinner, T. A. Kursar, R. F. Stallard, and S. J. Wright. 2006. The relative roles of environment, history and local dispersal in controlling the distributions of common tree and shrub species in a tropical forest landscape, Panama. Journal of Tropical Ecology 22:575–586.

Thomas, M. 1949. A generalization of Poisson's binomial limit for use in ecology. Biometrika 36:18–25.

Tilman, D., and P. Kareiva, eds. 1997. Spatial ecology: the role of space in population dynamics and interspecific interactions. Princeton University Press, Princeton.

Wehncke, E. V., S. P. Hubbell, R. B. Foster, and J. W. Dalling. 2003. Seed dispersal patterns produced by white-faced monkeys: implications for the dispersal limitation of Neotropical tree species. Journal of Ecology 91:677–685.

Wiegand, T., and K. A. Moloney. 2004. Rings, circles, and null-models for point pattern analysis in ecology. Oikos 104:209–229.

Wiegand, T., K. A. Moloney, J. Naves, and F. Knauer. 1999. Finding the missing link between landscape structure and population dynamics: a spatially explicit perspective. American Naturalist 154: 605–627.

Wiegand, T., F. Jeltsch, I. Hanski, and V. Grimm. 2003. Using pattern-oriented modelling for revealing hidden information: a key for reconciling ecological theory and application. Oikos 100:209–222.

Wiegand, T., S. Gunatilleke, N. Gunatilleke, and T. Okuda. 2007*a*. Analyzing the spatial structure of a Sri Lankan tree species with multiple scales of clustering. Ecology 88:3088–3102.

Wiegand, T., C. V. S. Gunatilleke, I. A. U. N. Gunatilleke, and A. Huth. 2007*b*. How individual species structure diversity in tropical forests. Proceedings of the National Academy of Sciences of the USA. 104:19029–19033.

———. 2007*c*. Species associations in a heterogeneous Sri Lankan dipterocarp forest. American Naturalist 170:E77–E95.

Associate Editor: Peter D. Taylor
Editor: Donald L. DeAngelis